A REVIEW OF NUMERICAL METHODS FOR NONLINEAR PARTIAL DIFFERENTIAL EQUATIONS

EITAN TADMOR

To Heinz-Otto Kreiss with friendship and appreciation

ABSTRACT. Numerical methods were first put into use as an effective tool for solving partial differential equations (PDEs) by John von Neumann in the mid-1940s. In a 1949 letter von Neumann wrote "the entire computing machine is merely one component of a greater whole, namely, of the unity formed by the computing machine, the mathematical problems that go with it, and the type of planning which is called by both." The "greater whole" is viewed today as scientific computation: over the past sixty years, scientific computation has emerged as the most versatile tool to complement theory and experiments, and numerical methods for solving PDEs are at the heart of many of today's advanced scientific computations. Numerical solutions found their way from financial models on Wall Street to traffic models on Main Street. Here we provide a bird's eye view on the development of these numerical methods with a particular emphasis on nonlinear PDEs.

CONTENTS

1. INTRODUCTION

Partial differential equations (PDEs) provide a quantitative description for many central models in physical, biological, and social sciences. The description is furnished in terms of unknown functions of two or more independent variables, and the relation between partial derivatives with respect to those variables. A PDE is said to be *nonlinear* if the relations between the unknown functions and their partial derivatives involved in the equation are nonlinear. Despite the apparent simplicity of the underlying differential relations, nonlinear PDEs govern a vast array of complex phenomena of motion, reaction, diffusion, equilibrium, conservation, and more. Due to their pivotal role in science and engineering, PDEs are studied extensively by specialists and practitioners. Indeed, these studies found their way into many entries throughout the scientific literature. They reflect a rich development of mathematical theories and analytical techniques to solve PDEs and illuminate the phenomena they govern. Yet, analytical theories provide only a limited account for the array of complex phenomena governed by nonlinear PDEs.

Over the past sixty years, scientific computation has emerged as the most versatile tool to complement theory and experiments. Modern numerical methods, in particular those for solving nonlinear PDEs, are at the heart of many of these advanced scientific computations. Indeed, numerical computations have not only joined experiment and theory as one of the fundamental tools of investigation, but they have also altered the kind of experiments performed and have expanded the scope of theory. This interplay between computation, theory, and experiments was envisioned by John von Neumann, who in 1949 wrote "the entire computing machine is merely one component of a greater whole, namely, of the unity formed by the computing machine, the mathematical problems that go with it, and the type of planning which is called by both" [156, p. 77]. Numerical solutions of nonlinear PDEs were first put into use in practical problems, by von Neumann himself, in the mid-1940s as part of the war effort. Since then, the advent of powerful computers combined with the development of sophisticated numerical algorithms has revolutionized science and technology, much like the revolutions that followed the introduction of the microscope and telescope in the seventeenth century. Powered by modern numerical methods for solving for nonlinear PDEs, a whole new discipline of numerical weather prediction was formed. Simulations of nuclear explosions replaced ground experiments. Numerical methods replaced wind tunnels in the design of new airplanes. Insight into chaotic dynamics and fractal behavior was gained only by repeating "computational experiments". Numerical solutions of nonlinear PDEs found their way from financial models on Wall Street to traffic models on Main Street.

In this review we provide a bird's eye view on the development of these numerical methods, with a particular emphasis on *nonlinear PDEs*. We begin in section 2 with a brief discussion of a few canonical examples of nonlinear PDEs, where

we make the usual distinction between two main classes of *boundary-value problems* and *time-dependent problems*. These examples serve as a concrete "platform" for our discussion on the construction, analysis and implementation of numerical methods for the approximate solution of nonlinear PDEs. In section 3 we demonstrate the construction and implementation of numerical methods in the context of the canonical PDEs mentioned above. Here, we focus attention on the four main classes of numerical methods: *finite-difference methods*, *finite-element methods*, *finite-volume methods*, and *spectral methods*. The limited scope of this review requires us to make a selection of topics; we chose to emphasize certain aspects of numerical methods pertaining to the nonlinear character of the underlying PDEs. In section 4 we discuss the basic concepts involved in the analysis of numerical methods: *consistency*, *stability*, and *convergence*. The numerical analysis of these concepts is fairly well understood in the linear setup. Again, we chose to highlight here the analysis of numerical methods in the nonlinear setup. Much like the theory of nonlinear PDEs, the numerical analysis of their approximate solutions is still a "work in progress".

We close this introduction with a brief glossary.

Variables, functions and vector functions. We use **boldface** letters to denote vectors, e.g., $w(\mathbf{x}) : \mathbb{R}^d \mapsto \mathbb{R}$ is a real-valued function of the d-vector variables $\mathbf{x} = (x_1, \ldots, x_d) \in \mathbb{R}^d$, and $\mathbf{w}(\mathbf{x}) : \mathbb{R}^d \mapsto \mathbb{R}^p$ is a p-vector function in $\mathbf{x}$. Similarly, $\mathbf{w_j}$ denotes a gridfunction defined at Cartesian gridpoints, $\mathbf{x_j} = (j_1 \Delta x_1, \ldots, j_d \Delta x_d)$, where $\Delta x = (\Delta x_1, \ldots, \Delta x_d)$ is the mesh size and $\mathbf{j} = (j_1, \ldots, j_d) \in \mathbb{Z}^d$ denotes a d-vector of indices of size $|\mathbf{j}| = \sum j_k$. The Euclidean ℓ^2-product and norm are denoted by $\langle \mathbf{w}, \mathbf{v} \rangle = \sum_j u_j v_j$ and $|\mathbf{w}|^2 = \langle \mathbf{w}, \mathbf{w} \rangle$, respectively. We let $\widehat{\mathbf{w}}(\mathbf{k})$ denote the Fourier coefficients of $\mathbf{w}(\mathbf{x})$.

Geometry. We use Ω as a generic notation for a connected domain in $\mathbb{R}^d$ with a smooth boundary $\partial\Omega$, and we let $\mathbf{1}_\Omega$ denote its characteristic function

$$\mathbf{1}_\Omega(x) = \begin{cases} 1 & x \in \Omega, \\ 0 & x \notin \Omega. \end{cases}$$

We let Ω_Δ denote different discretizations of Ω, which are identified by one or more small discretization parameters, Δ. For example, a Cartesian grid, $\{\mathbf{x_j} \mid \mathbf{x_j} \in \Omega\}$ with small cells of length $\Delta := \sum_j \Delta x_j$, a triangulation of a two-dimensional domain, $\Omega = \bigcup_j T_j$ of small size $\Delta := \max_j \operatorname{diam} T_j$, etc., $\partial\Omega_\Delta$ denotes the discrete boundary, i.e., the elements of Ω_Δ that are not fully enclosed inside the interior of Ω.

Differential and difference operators. We abbreviate $\partial^{\mathbf{j}} := \partial_{x_1}^{j_1} \partial_{x_2}^{j_2} \cdots \partial_{x_d}^{j_d}$, to denote a partial differentiation of order $|\mathbf{j}|$. L^p denotes the usual Lebesgue spaces and $W^m(L^p)$ denotes the Sobolev space, $\{w \mid \sum_{|\mathbf{j}| \le m} \|\partial^{\mathbf{j}} w\|_{L^p} < \infty\}$ for $m = 1, 2, \ldots$, and is defined by duality for $m = -1, -2, \ldots$, with the necessary modifications for $p = 1, \infty$. The important special case $p = 2$ is often encountered with its own special notation of Sobolev space H^m and its zero trace subspace H_0^m [150, 1]. The gradient of $w(\mathbf{x})$ is the d-vector of its first derivatives, $\nabla w := (\partial_1 w, \ldots, \partial_d w)$; in particular, $\partial_{\mathbf{n}} w = \nabla w \cdot \mathbf{n}$ denotes differentiation in a normal direction $\mathbf{n}$, and $\frac{d}{dx} w(x) \equiv w'(x)$ denotes univariate differentiation. The Hessian, $\mathcal{D}^2 w$, is the $d \times d$ matrix consisting of the second derivatives, $\mathcal{D}^2 w := \{\partial_{jk} w\}_{j,k=1}^d$, and its trace is the Laplacian, $\Delta w = \sum_{j=1}^d \partial_j^2 w$. We use UPPERCASE letters to identify numerical approximations of

(vector) functions, which are denoted by the corresponding lowercase letters, e.g., $\mathbf{W}(\mathbf{x}), C_\mathbf{j}, \ldots$ are viewed as approximations of $\mathbf{w}(\mathbf{x}), c(\mathbf{x_j}), \ldots$, etc. We let $D_{\pm x_j}$ denote the divided difference operator

$$D_{\pm x_k}\mathbf{W_j} = \pm\frac{\mathbf{W}_{j_1,\ldots,j_k\pm 1,\ldots,j_d} - \mathbf{W_j}}{\Delta x_k}.$$

Finally, $X \approx Y$ indicates that $X - Y \to 0$ as the small discretization parameter $\Delta \downarrow 0$, and we use $X \lesssim Y$ to denote the estimate $X \leq CY$, where C is a constant which may depend on $\mathbf{w}(\cdot), \mathbf{W}(\cdot)$, and their derivatives, divided differences, etc., but is independent of Δ.

2. Examples of nonlinear PDEs

We consider nonlinear PDEs, which take the form

$$(2.1) \qquad \mathcal{A}\big(\partial^{\mathbf{s}}\mathbf{w}, \partial^{\mathbf{s}-1}\mathbf{w}, \ldots, \partial\mathbf{w}, \mathbf{w}, \mathbf{x}\big) = \mathbf{g}(\mathbf{x}).$$

Here, $\mathbf{w} := (w_1(\mathbf{x}), \ldots, w_p(\mathbf{x})) : \Omega \mapsto \mathbb{R}^p$ is the vector of p unknown functions of the independent variables, $\mathbf{x} := (x_1, \ldots, x_d) \in \Omega \subset \mathbb{R}^d_{\mathbf{x}}$, and $\mathbf{g} : \Omega \mapsto \mathbb{R}^p$ is given. If time is involved as one of the independent variables, it is customary to identify it as the zeroth variable, $x_0 = t$. The highest derivative involved, $s = |\mathbf{s}|$, determines the *order* of the equation. The equation is *nonlinear* if $\mathcal{A}$ is nonlinear in $\mathbf{w}$ or any of its s partial derivatives. Often, nonlinear PDEs involve one or more small parameters, which dictate the *multiscale* character of the nonlinear problem. Below, we identify such parameters with typical notations of $\hbar, \epsilon, \nu, \lambda, \kappa$, etc. A few examples are in order.

2.1. **Examples of boundary-value PDEs.** We begin with a canonical example of the first-order Eikonal equation,

$$(2.2) \qquad |\nabla_{\mathbf{x}}w| = g(\mathbf{x}), \qquad w : \Omega \mapsto \mathbb{R}, \quad \Omega \subset \mathbb{R}^2_{\mathbf{x}}.$$

Equation (2.2) arises in several different contexts, notably in *geometrical optics*, *optimal control*, and *computer vision* [74, 76, 183, 171]. It is the forerunner for the large class of nonlinear Hamilton–Jacobi equations whose solution, properly interpreted [57], is uniquely determined by the prescribed boundary values, $w(\mathbf{x}) = b(\mathbf{x})$, $\mathbf{x} \in \partial\Omega$.

We continue with a prototype nonlinear PDE which arises in *geometry*,

$$(2.3\text{a}) \qquad \nabla_{\mathbf{x}} \cdot \Big(\frac{\nabla_{\mathbf{x}}w}{\sqrt{1 + |\nabla_{\mathbf{x}}w|^2}}\Big) = g(\mathbf{x}), \qquad w : \Omega \mapsto \mathbb{R}, \quad \Omega \subset \mathbb{R}^2_{\mathbf{x}}.$$

Here, we seek a solution $w \equiv w(\mathbf{x})$ defined over a domain Ω (which for simplicity is assumed to be convex), whose graph has the given mean curvature, $g : \Omega \mapsto \mathbb{R}$, and is subject to Dirichlet boundary conditions, $w(\mathbf{x}) = b(\mathbf{x})$, $\mathbf{x} \in \partial\Omega$. When $g = 0$, (2.3a) is the *minimal surface equation* [70, 170, 34, 76], whose solution is identified as the minimizer of the surface area

$$(2.3\text{b}) \qquad w = \arg\min_u \Big\{ \int_\Omega \sqrt{1 + |\nabla_{\mathbf{x}}u|^2}\, d\mathbf{x} \;\Big|\; u_{|\partial\Omega} = b\Big\}.$$

The minimal surface equation is an example of a nonlinear second-order PDE of *elliptic type* [88, 30, 99].

Another example of a nonlinear system of PDEs encountered in the context of *image processing* is the degenerate elliptic equation [165, 2, 178],

$$(2.4) \qquad \mathbf{w} - \lambda \nabla_{\mathbf{x}} \cdot \left(\frac{\nabla_{\mathbf{x}} \mathbf{w}}{|\nabla_{\mathbf{x}} \mathbf{w}|} \right) = \mathbf{g}(\mathbf{x}), \qquad \mathbf{w} : \Omega \subset \mathbb{R}_{\mathbf{x}}^2 \mapsto \mathbb{R}^3.$$

This system of equations governs a 3-vector, $\mathbf{w} \equiv \mathbf{w}(\mathbf{x})$, which measures the intensity of red, green, and blue pixels in a colored image. Given a noisy image, $\mathbf{g} \equiv \mathbf{g}(\mathbf{x}) : \Omega \mapsto \mathbb{R}^3$, the purpose is to find its denoised version, $\mathbf{w}(\mathbf{x})$, by diffusing the noise in directions parallel to the image edges. Here, $\lambda > 0$ is a diffusive scaling parameter which may depend on $|\nabla_{\mathbf{x}} \mathbf{w}|$. Similarly to the minimal surface equation, (2.4) can be derived from an appropriate *variational principle*. It is augmented with a Neumann-type boundary condition, $\partial_{\mathbf{n}} \mathbf{w}_{|\partial \Omega} = 0$.

An example of a fully nonlinear elliptic PDE is encountered in *optimal transport problems*, which are governed by the *Monge–Ampère equation* [29, 218],

$$(2.5) \qquad \text{Det} \, \mathcal{D}^2 w = Q(\mathbf{x}, w, \nabla_{\mathbf{x}} w), \qquad w : \Omega \mapsto \mathbb{R}, \quad \Omega \subset \mathbb{R}_{\mathbf{x}}^d.$$

Here, $w \equiv w(\mathbf{x})$ is the convex potential whose gradient, $\nabla_{\mathbf{x}} w$, maps the optimal transportation path and is subject to Dirichlet-type boundary conditions, $w(\mathbf{x}) = b(\mathbf{x})$, $\mathbf{x} \in \partial \Omega$.

2.2. Examples of time-dependent PDEs.

Atomic physics is dominated by the *Schrödinger equation*

$$(2.6) \qquad i\hbar \partial_t \mathbf{w} + \frac{\hbar^2}{2m} \Delta \mathbf{w} - V(\mathbf{w})\mathbf{w} = 0, \qquad \mathbf{w} : \mathbb{R}_{t \geq t_0} \times \mathbb{R}_{\mathbf{x}}^d \mapsto \mathbb{C}.$$

The equation governs a complex-valued wavefunction, $\mathbf{w} \equiv \mathbf{w}(t, \mathbf{x})$, associated with a particle of mass m and driven by a potential $V(\mathbf{w})$. Starting with a given initial state, $\mathbf{w}(t_0, \mathbf{x}) = \mathbf{f}(\mathbf{x})$, a solution $\mathbf{w}(t, \mathbf{x})$ is sought for $t > t_0$. The equation is *semilinear* in the sense that its nonlinearity involves only $\mathbf{w}$ but no higher derivatives. It depends on a quantum scale, dictated by the small Planck's constant $\hbar \sim 10^{-34}$. As another example of a semilinear PDEs with a pivotal role in mathematical physics, we mention the *Boltzmann equation* [67, 35], which provides a microscopic description of the dynamics of many particles in dilute gases.

Turning to models on the "human scale", we consider as a prototype the one-dimensional system of *convection-diffusion* equations,

$$(2.7a) \qquad \partial_t \mathbf{w} + \partial_x \mathbf{F}(\mathbf{w}) - \nu \partial_x \mathbf{Q}(\partial_x \mathbf{w}) = \mathbf{g}(t, x), \qquad \mathbf{w} : \mathbb{R}_{t \geq t_0} \times \Omega \mapsto \mathbb{R}^p,$$

defined over an interval $\Omega \subset \mathbb{R}_x$. It is complemented by prescribed initial values, $\mathbf{w}(t_0, x) = \mathbf{f}(x)$, and appropriate boundary conditions along $\mathbb{R}_{t \geq t_0} \times \partial \Omega$. Many models in *fluid dynamics* and *elasticity theory* are governed by convection-diffusion equations which involve a p-vector of conserved quantities, $\mathbf{w} \equiv \mathbf{w}(t, x)$, such as density, momentum, total energy, etc. Their convection is governed by the nonlinear flux, $\mathbf{F}(\mathbf{w}) := (F_1(\mathbf{w}), \dots, F_p(\mathbf{w}))$, and $\mathbf{Q}(\partial_x \mathbf{w}) := (Q_1(\partial_x \mathbf{w}), \dots, Q_p(\partial_x \mathbf{w}))$ represents various diffusive mechanisms such as viscosity, heat conductivity, etc. Often, diffusion enters the problem with a small amplitude, $\nu \approx 0$. The p-vector functions $\mathbf{g} \equiv \mathbf{g}(t, x)$, models different source terms. When $\nu = 0$, (2.7a) is reduced to

$$(2.7b) \qquad \partial_t \mathbf{w} + \partial_x \mathbf{F}(\mathbf{w}) = \mathbf{g}(t, x), \qquad \mathbf{w} : \mathbb{R}_{t \geq t_0} \times \Omega \mapsto \mathbb{R}^p, \quad \Omega \subset \mathbb{R}_x.$$

This is a first-order system of balance laws of *hyperbolic type*, assuming that the eigenvalues of the Jacobian matrix, $\mathbf{F}_{\mathbf{w}}(\mathbf{w})$, are real; in the particular case $\mathbf{g} = 0$,

it is a system of conservation laws [182, 59, 131]. When diffusion is added, $\nu > 0$, the second-order system (2.7a) is of *parabolic type*, assuming the diffusion matrix is positive, $\mathbf{Q_w(w)} > 0$ [81, 187, 125]. In either case, (2.7a), (2.7b) are examples of *quasilinear* PDEs, in the sense that they depend linearly on the highest derivative appearing in the equation, whether $\nu > 0$ or $\nu = 0$.

The compressible *Navier–Stokes equations* [56, 140] provide a macroscopic description of gases; the incompressible Navier–Stokes equations [51, 139, 144, 124] govern a macroscopic dynamics of liquids. These are the most important examples for multidimensional convection-diffusion equations, with a vast literature on their numerical solution. When viscosity effects are neglected, one obtains the *Euler equations*. As an example, we record here the rotational shallow-water equations [163, 145]. Expressed in terms of the 3-vector, $\mathbf{w} = (h, \mathbf{v})$, where $\mathbf{v} = (v_1, v_2)$ are the velocity components in the $\mathbf{x} = (x_1, x_2)$-coordinates, $\mathbf{x} \in \Omega \subset \mathbb{R}^2_{\mathbf{x}}$, and h is the total height of the flow (which is assumed shallow relative to the horizontal $\mathbf{x}$ scales), the systems of equations read

$$(2.8a) \quad \partial_t \mathbf{w} + (\mathbf{v} \cdot \nabla_{\mathbf{x}})\mathbf{w} + \begin{bmatrix} h\nabla_{\mathbf{x}} \cdot \mathbf{v} \\ gh_{x_1} \\ gh_{x_2} \end{bmatrix} + f \begin{bmatrix} 0 \\ -v_2 \\ v_1 \end{bmatrix} = 0, \qquad \mathbf{w} : \mathbb{R}_{t \geq t_0} \times \Omega \mapsto \mathbb{R}^3.$$

Here g is the acceleration gravity and f is the Coriolis parameter which signifies the rotation frequency. If we neglect the variations in h, then by taking the *curl* of (2.8a) we find that $w := \partial_{x_1} v_2 - \partial_{x_2} v_1$ satisfies the *vorticity equation* associated with the inviscid Euler equations,

$$(2.8b) \qquad\qquad\qquad \partial_t w + \mathbf{v} \cdot \nabla_{\mathbf{x}} w = 0.$$

The divergence-free velocity field, $\mathbf{v(x)} = (-\partial_{x_2}, \partial_{x_1})\Delta^{-1} w(\mathbf{x})$, reflects the incompressibility of the flow.

Our next example of a multidimensional convection-diffusion equation is drawn from the *biological literature*: the *chemotaxis model* [119, 106, 78, 104] is given by,

$$(2.9a) \qquad \partial_t w + \kappa \nabla_{\mathbf{x}} \cdot \left(w \nabla_{\mathbf{x}} c \right) - \Delta_{\mathbf{x}} w = 0, \qquad w : \mathbb{R}_{t \geq t_0} \times \Omega \mapsto \mathbb{R}, \quad \Omega \subset \mathbb{R}^2_{\mathbf{x}}.$$

Here, $w \equiv w(t, \mathbf{x})$ represents the scalar density of bacteria or amoebae cells that have drifted due to a chemo-attractant with concentration $c \equiv c(t, \mathbf{x})$. The drift or convection is modeled by the flux, $\mathbf{F}(w) = w\nabla_{\mathbf{x}} c$, where concentration is coupled to the density through the Poisson's equation,

$$(2.9b) \qquad\qquad \Delta_{\mathbf{x}} c = -w, \qquad c : \mathbb{R}_{t \geq t_0} \times \Omega \mapsto \mathbb{R}.$$

Equation (2.9) is augmented with initial conditions, $w(t_0, \mathbf{x}) = f(\mathbf{x})$, and Neumann-type boundary conditions, $\partial_{\mathbf{n}} u(t, \mathbf{x}) = \partial_{\mathbf{n}} c(t, \mathbf{x}) = 0$, $\mathbf{x} \in \partial\Omega$. The parameter $\kappa > 0$ quantifies the sensitivity by measuring the nonlinearity in the system.

We conclude with an example from *topology*. The *Ricci flow*, introduced by Hamilton [98] and used by Perelman [164, 153] to solve the Poincaré conjecture, takes the form

$$(2.10) \qquad\qquad \partial_t \mathbf{w}_{\alpha\beta} = 2\,\mathrm{Ric}_{\alpha\beta}(t, \mathbf{x}), \qquad \mathbf{w} : \mathbb{R}_{t \geq 0} \times \mathcal{M} \mapsto \mathbb{R}^{3 \times 3}.$$

Here the unknown $\mathbf{w} \equiv \mathbf{w}_{\alpha\beta}(t, \mathbf{x})$ is a 3×3 time-dependent array of a Riemannian metric on a manifold $\mathcal{M}$, and $\mathrm{Ric} = \mathrm{Ric}_{\alpha\beta}$ is the Ricci curvature tensor associated with $\mathcal{M}$.

2.3. **Well-posed problems.** Nonlinear PDEs such as the equations mentioned above are to be augmented with boundary conditions, where the values of the unknown $\mathbf{w}(\cdot)$ and/or of its derivatives are prescribed along the boundary of the domain Ω. In particular, time-dependent problems are augmented with initial values prescribed at the initial time, $t = t_0$. Additional auxiliary conditions, such as closure relations, entropy conditions, regional invariance, etc., are often required to complement the full statement of nonlinear PDEs. The combination of one or more nonlinear PDEs, augmented with prescribed initial and boundary conditions together with necessary auxiliary conditions, form the typical "problem" we are interested in. It is assumed that the problem is *well posed*, in the sense of satisfying the following three conditions:

(i) It admits a solution.
(ii) This solution is unique; thus, there exists a well-defined *solution operator*, which maps the boundary data $\mathbf{b}(\cdot)$, the inhomogeneous data $\mathbf{g}(\cdot)$, and, in the time-dependent problem, the initial data $\mathbf{w}_0(\cdot)$, to *the* solution $\mathbf{w}(\cdot)$:

$$\{\mathbf{g}(\cdot), \mathbf{b}(\cdot)\} \mapsto \mathbf{w}(\cdot) \quad \text{or} \quad \{\mathbf{w}_0(\cdot), \mathbf{g}(t, \cdot), \mathbf{b}(t, \cdot)\} \mapsto \mathbf{w}(t, \cdot).$$

(iii) The solution operator depends *continuously* on the prescribed initial, boundary, and inhomogeneous data.

This notion of well-posedness requires a proper notion of solution and a proper metric to quantify its continuous dependence on the data. We shall not discuss these issues here except for noting that the theory of nonlinear PDEs is still very much a "work in progress". We refer to [57, 30, 207, 76, 139, 140, 182, 59, 204] and the references therein for examples of such recent work.[1] Indeed, two out of the remaining six open problems offered as the "Millennium Problems" by the Clay Institute [46] have their roots in nonlinear PDEs—the Navier–Stokes equations and the Yang–Mills theory. A seventh Clay problem of the Poincaré conjecture was proved by PDE tools; consult [203]. Numerical methods provide a quantitative and qualitative insight for problems governed by nonlinear PDEs, a complementary avenue to the theoretical studies of such problems.

3. Numerical methods

There is a variety of different numerical methods for the approximate solution of nonlinear PDEs. These methods are classified according to their representation of approximate solutions. We shall mention the four main ones, beginning with the oldest [55].

3.1. **Finite-difference methods.** *Finite-difference methods* consist of a discrete grid, $\Omega_\Delta := \{\mathbf{x_j}\}$, and a gridfunction, $\mathbf{W}_\Delta := \{\mathbf{W_j}\}$. The grid Ω_Δ is a graph of discrete gridpoints $\mathbf{x_j} \in \Omega \subset \mathbb{R}^d_{\mathbf{x}}$ and a certain set of their neighbors, $\mathbf{x_{j_k}}$, $\mathbf{j}_k \in \mathcal{N}(\mathbf{j})$. The vectors $\{\mathbf{x_j} - \mathbf{x_{j_k}}\}_{\mathbf{j}_k \in \mathcal{N}(\mathbf{j})}$ form the *stencil* associated with $\mathbf{x_j}$. Here, Δ abbreviates one or more discretization parameters of the underlying grid, Ω_Δ, which measure the clustering of these neighbors: the smaller Δ is, the closer $\mathbf{x_{j_k}}$ are to $\mathbf{x_j}$. Divided differences along appropriate discrete stencils are used to approximate the partial derivatives of the PDE (2.1). The resulting relations between the divided differences form a *finite-difference scheme*. Its solution, $\{\mathbf{W_j}\}$, is sought as an

---

[1]Our bibliography does not intend to be comprehensive but to provide a mixture of classic and modern references.

approximation to the *pointvalues* of the exact solution of the PDE (2.1), $\{\mathbf{w}(\mathbf{x_j})\}$, as we refine the grid by letting $\Delta \downarrow 0$. Finite-difference methods provide a versatile tool for the numerical solution of PDEs: their derivation in terms of divided differences is straightforward, they are easy to implement, and they appeal to the full spectrum of linear and nonlinear PDEs.

The typical framework of finite-difference methods is based on *Cartesian grids* of equispaced gridpoints. As a concrete example, we will consider two-dimensional spatial variables, which are conveniently relabeled as $(x, y) \in \Omega \subset \mathbb{R}_x \times \mathbb{R}_y$. The domain Ω is covered with a Cartesian grid, $\Omega_\Delta = \{(x_j, y_k) := (j\Delta x, k\Delta y) \in \Omega\}$. A gridfunction, $\{\mathbf{W}_{jk}, \ (x_j, y_k) \in \Omega_\Delta\}$, is sought as an approximation for the corresponding *pointvalues* of an exact solution, $\mathbf{w}_{jk} := \mathbf{w}(x_j, y_k)$, as $\Delta := |\Delta x| + |\Delta y|$ tends to zero. The gridfunction $\{\mathbf{W}_{jk}\}$ is obtained as the solution of an appropriate finite-difference scheme. The construction of such schemes proceeds by replacing partial derivatives with approximate divided differences. For example, one may use

$$\text{(3.1)} \quad D_{+x}\mathbf{W}_{jk} := \frac{\mathbf{W}_{j+1,k} - \mathbf{W}_{jk}}{\Delta x}, \quad D_{-y}\mathbf{W}_{jk} := \frac{\mathbf{W}_{jk} - \mathbf{W}_{j,k-1}}{\Delta y},$$
$$D_{0x}\mathbf{W}_{jk} := \frac{\mathbf{W}_{j+1,k} - \mathbf{W}_{j-1,k}}{2\Delta x},$$

where D_{+x}, D_{-y}, D_{0x} are standard *difference operators* based on forward, backward, and a centered stencils, which enable us to abbreviate the lengthy formulation of finite-difference schemes. There is a large variety of such difference operators to approximate first- and higher-order derivatives.

We now put these ingredients into the construction of a finite-difference approximation for the Eikonal equation (2.2),

$$\text{(3.2a)} \qquad |\nabla W_{jk}| = g(x_j, y_k), \quad (x_j, y_k) \in \Omega_\Delta,$$

where ∇W_{jk} stands for a approximate gradient,

$$\text{(3.2b)} \quad \nabla W_{jk} = \Big(\max\{D_{-x}W_{jk}, -D_{+x}W_{jk}, 0\}, \ \max\{D_{-y}W_{jk}, -D_{+y}W_{jk}, 0\} \Big).$$

The reason for this judicious choice of divided differences in (3.2b) is tied to the fact that the underlying Eikonal solution sought in (2.2) is not necessarily differentiable.

In a similar manner, we discretize the minimal surface equation (2.3a),

(3.3)
$$D_{+x}\left(\frac{D_{-x}W_{jk}}{\sqrt{1 + |\nabla_- W_{jk}|^2}} \right) + D_{+y}\left(\frac{D_{-y}W_{jk}}{\sqrt{1 + |\nabla_- W_{jk}|^2}} \right) = g(x_j, y_k), \quad (x_j, y_k) \in \Omega_\Delta.$$

Here we set $|\nabla_- W_{jk}|^2 = |D_{-x}W_{jk}|^2 + |D_{-y}W_{jk}|^2$, using backward differences to discretize the gradient. The finite-difference scheme (3.3) is complemented by the prescribed boundary values, $W_{jk} = b(x_j, x_k), (x_j, y_k) \in \partial\Omega_\Delta$.

A similar finite-difference discretization of the denoising model (2.4) reads

$$\text{(3.4)} \quad \mathbf{W}_{jk} - \lambda \left[D_{-x}\left(\frac{D_{+x}\mathbf{W}_{jk}}{\sqrt{\epsilon^2 + |\nabla_+ \mathbf{W}_{jk}|^2}} \right) + D_{-y}\left(\frac{D_{+y}\mathbf{W}_{jk}}{\sqrt{\epsilon^2 + |\nabla_+ \mathbf{W}_{jk}|^2}} \right) \right]$$
$$= (x_j, y_k), (x_j, y_k) \in \Omega_\Delta.$$

A small parameter, $0 < \epsilon \ll \Delta$, was introduced to avoid the singularity of the discrete gradient in the denominators on the left; note that this time we chose to discretize the gradient using forward biased differencing. The finite-difference

FIGURE 3.1. Five-point stencil $(0-4)$, seven-point stencil $(0-6)$, and nine-point stencil $(0-8)$.

scheme (3.4) is complemented by the prescribed normal derivatives, $D_{\mathbf{n}}\mathbf{W}_{jk}$, whenever $(x_j, y_k) \in \partial\Omega_\Delta$.

The finite-difference schemes (3.2), (3.3), and (3.4) amount to nonlinear systems of *algebraic equations*, $\mathbb{A}(\mathbf{W}_\Delta) = \mathbf{G}_\Delta$, for the unknowns, $\mathbf{W}_\Delta = \{\mathbf{W}_{jk}\}$. The systems are *sparse* in the sense that each unknown, W_{jk} or $\mathbf{W}_{jk}$, is connected only to its immediate neighboring gridvalues, depicted in Figure 3.1. The solution strategy for such systems is often tied to the nature of the underlying PDEs. Thus for example, the stencil of Eikonal solver (3.2) involves at most five neighboring gridpoints. The one-sided differences in (3.2) propagate information in the "upwind" directions, namely, from the prescribed boundary data, $W_{jk} = b(x_j, y_k)_{|(x_j, y_k) \in \partial\Omega_\Delta}$, into the interior of the computational domain, Ω_Δ. The resulting algebraic equations, $\mathbb{A}(\mathbf{W}_\Delta) = \mathbf{G}_\Delta$, can be solved efficiently by the *fast marching method* [183]. The stencils on the left of (3.3) and (3.4) involve seven gridpoints and are not symmetric; to avoid the lack of symmetry, one may alternate between forward and backward biased stencils, which ends up with a symmetric stencil based on nine neighboring gridpoints. The solution of sparse algebraic systems that arises from discretizations of elliptic equations such as (3.3) and (3.4) is accomplished by standard iterative solvers [92, 215, 179]. There are several major approaches that take advantage of the intimate relation between the algebraic system and its underlying boundary-value PDE: we mention in this context the important classes of *multigrid methods* and the *fast multipole methods* [24, 94, 219] as the forerunners for a vast literature. Figure 3.2 demonstrates the successive solution of (3.4) for hierarchical decomposition of an MRI image.

FIGURE 3.2. Hierarchical decomposition of an MRI image [200]. Starting with the image, $\mathbf{W}^0$ on the left, the figure shows its successive decompositions, $\sum_{n=0}^{m}\mathbf{W}^n$, $m = 3, 4, 5, 6$, where $\mathbf{W}^n$ is the solution of (3.4) with $\lambda = 4^{m-1} \cdot 10^{-3}$ and $\mathbf{g} \mapsto \mathbf{W}^{n-1}$.
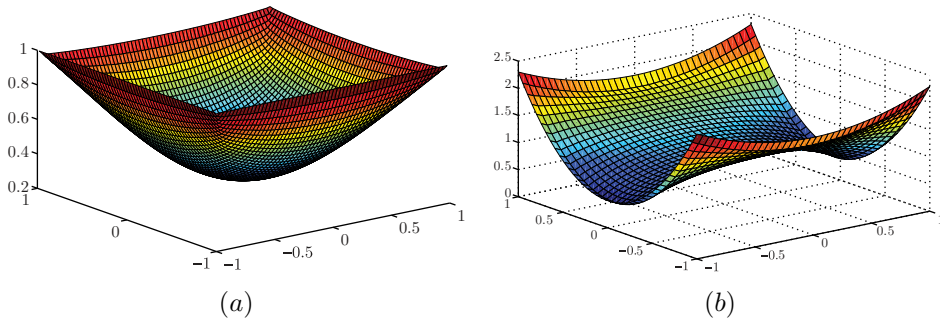
FIGURE 3.3. A finite-difference approximation based on a 17-point stencil (3.5b). (a) A finite-difference solution (3.5a) of the Monge–Ampère equation $\operatorname{Det} \mathcal{D}^2 w(x) = 1$ on $\Omega =$ the unit square, subject to the boundary condition, $w(\mathbf{x}) = 1$, $\mathbf{x} \in \partial\Omega$. (b) A finite-difference solution of Pucci problem, $2\lambda_-(\mathcal{D}^2 w(x)) + \lambda_+(\mathcal{D}^2 w(x)) = 0$, subject to the boundary condition, $w(\mathbf{x}) = x_1^2 - x_2^2$, $\mathbf{x} \in \partial\Omega$.

We turn to examine a finite-difference approximation of the two-dimensional Monge–Ampère equation (2.5), which is expressed in terms of the eigenvalues of $\mathcal{D}^2 W$,

$$(3.5a) \qquad \lambda_-(\mathcal{D}^2 W_{\mathbf{j}})\lambda_+(\mathcal{D}^2 W_{\mathbf{j}}) = Q(\mathbf{x_j}, W_{\mathbf{j}}, D_{0x} W_{\mathbf{j}}, D_{0y} W_{\mathbf{j}}).$$

To evaluate the eigenvalues on the left, one employs a Rayleigh–Ritz characterization of the smallest and largest eigenvalues of $\mathcal{D}^2 W$,

$$(3.5b) \qquad \left\{ \begin{array}{c} \lambda_-(\mathcal{D}^2 W_{\mathbf{j}}) \\ \lambda_+(\mathcal{D}^2 W_{\mathbf{j}}) \end{array} \right\} \approx \left\{ \begin{array}{c} \min_{\mathbf{k}} \\ \max_{\mathbf{k}} \end{array} \right\} \frac{W_{\mathbf{j}+\mathbf{j_k}} - 2W_{\mathbf{j}} + W_{\mathbf{j}-\mathbf{j_k}}}{|\Delta \mathbf{x_{j_k}}|^2},$$

where the $\min_{\mathbf{k}}$ and $\max_{\mathbf{k}}$ scan a predetermined stencil of gridpoints such that $\mathbf{x_j} \pm \Delta \mathbf{x_{j_k}} \in \Omega_\Delta$. The resulting nonlinear algebraic equations, $\mathbb{A}(\mathbf{W}_\Delta) = \mathbf{G}_\Delta$, can be solved by iterations: a numerical example of [158] is provided in Figure 3.3.

Next, we turn our attention to finite-difference methods for time-dependent problems. Here we seek gridfunctions, $\{\mathbf{W}_{jk}^n\}$, defined on a space-time Cartesian grid, $(t^n, x_j, y_k) := (n\Delta t, j\Delta x, k\Delta y)$. As an example, we consider a finite-difference approximation of the Schrödinger equation (2.6),

$$(3.6) \qquad \mathbf{W}_{jk}^{n+1} = \mathbf{W}_{jk}^n + i\frac{\hbar \Delta t}{2m}\Big(D_{+x}D_{-x} + D_{+y}D_{-y}\Big)\mathbf{W}_{jk}^n - i\frac{\Delta t}{\hbar}V\big(\mathbf{W}_{jk}^n\big)\mathbf{W}_{jk}^n.$$

One starts with prescribed initial conditions, $\mathbf{W}_{jk}^0 = \mathbf{f}(x_j, y_k)$, and uses the difference scheme (3.6) to compute the discrete wavefunction by advancing from one time level, $\mathbf{W}^n := \{\mathbf{W}_{jk}^n\}$, to the next, $\mathbf{W}^{n+1}$.

Similarly, the computation of a finite-difference approximation of convection-diffusion equations (2.7) or (2.8) advances in discrete time steps. For example, a difference scheme for (2.7a) takes the form

$$(3.7) \qquad \begin{aligned} \mathbf{W}_j^{n+1} = {} & \mathbf{W}_j^n - \frac{\Delta t}{2\Delta x}\Big(\mathbf{F}(\mathbf{W}_{j+1}^n) - \mathbf{F}(\mathbf{W}_{j-1}^n)\Big) \\ & + \nu\frac{\Delta t}{\Delta x}\Big(\mathbf{Q}\big(D_+\mathbf{W}_j^n\big) - \mathbf{Q}\big(D_-\mathbf{W}_j^n\big)\Big) + \Delta t \mathbf{G}_j^n. \end{aligned}$$
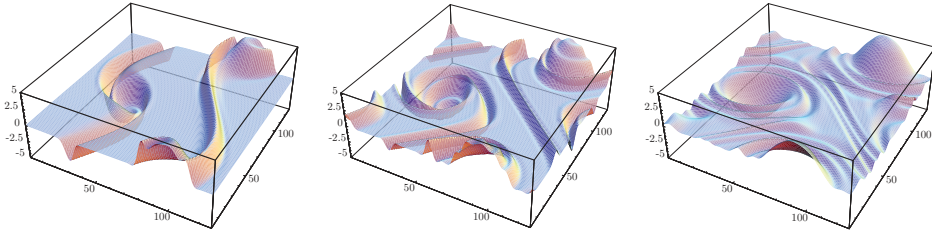
FIGURE 3.4. The time evolution of vorticity in two-dimensional inviscid Euler equations (2.8b) using a central difference scheme [137] computed at $t = 4, 6$ and $t = 10$.

Figure 3.4 demonstrates a finite-difference computation of the vorticity equation (2.8b).

Often, one is interested in discretizing only the spatial variables. For example, a finite-difference discretization of the two-dimensional chemotaxis problem (2.9) reads

(3.8)
$$\frac{d}{dt}W_{\mathbf{j}} = -\kappa\Big(D_{+x}\big(W_{\mathbf{j}}D_{-x}C_{\mathbf{j}}\big) + D_{+y}\big(W_{\mathbf{j}}D_{-y}C_{\mathbf{j}}\big)\Big) + \Big(D_{+x}D_{-x} + D_{+y}D_{-y}\Big)W_{\mathbf{j}}.$$

Here, $W_{\mathbf{j}} \equiv W_{(j_1,j_2)}(t)$ are the approximate densities at the gridpoints $\mathbf{x}_{\mathbf{j}} \in \Omega_\Delta$. The missing boundary values $\{W_{\mathbf{j}}(t), \mathbf{x}_{\mathbf{j}} \in \partial\Omega_\Delta\}$ are recovered from the Neumann-type boundary conditions $D_{\mathbf{n}}W_{\mathbf{j}}(t) = 0$. The approximate concentrations $C_{\mathbf{j}} \equiv C_{j_1,j_2}(t)$ are obtained as a finite-difference solution of the Poisson equation (2.9b), based on the standard five-point stencil

$$
\begin{array}{llrll}
\text{interior scheme}: & \big(D_{+x}D_{-x} + D_{+y}D_{-y}\big)C_{\mathbf{j}}(t) & = & -W_{\mathbf{j}}(t), & \mathbf{x}_{\mathbf{j}} \in \Omega_\Delta, \\
\text{boundary conditions}: & D_{\mathbf{n}}C_{\mathbf{j}} & = & 0, & \mathbf{x}_{\mathbf{j}} \in \partial\Omega_\Delta.
\end{array}
$$

In this fashion, one ends up with a semidiscrete approximation (3.8), called the *method of lines*, which amounts to a nonlinear system of ordinary differential equations (ODEs) for the unknowns $\{W_{\mathbf{j}}(t)\}$. The solution of such semidiscrete systems is obtained by standard ODE solvers [82, 96, 97, 28].

The finite-difference schemes (3.2)–(3.8) are typical examples of finite-difference approximations of nonlinear PDEs. The general recipe for such schemes can be expressed in terms of divided difference operators of order $\mathbf{j}$, $D_\Delta^{\mathbf{j}} = D_{+x_1}^{j_1} D_{+x_2}^{j_2} \cdots D_{+x_d}^{j_d}$, which are supported on the computational grid Ω_Δ. A finite-difference approximation of the PDE (2.1) is obtained by replacing the nonlinear relations between partial derivatives of $\mathbf{w}$ in (2.1) with similar relations between divided differences of the gridfunction, $\mathbf{W}_\Delta$,

(3.9) $\quad \mathcal{A}(D_\Delta^{\mathbf{s}}\mathbf{W}_{\mathbf{j}}, D_\Delta^{\mathbf{s}-1}\mathbf{W}_{\mathbf{j}}, \ldots, D_\Delta\mathbf{W}_{\mathbf{j}}, \mathbf{W}_{\mathbf{j}}, \mathbf{x}_{\mathbf{j}}) = \mathbf{G}_{\mathbf{j}},$

$$\mathbf{x}_{\mathbf{j}} = (x_{j_1}, x_{j_2}, \ldots, x_{j_d}) \in \Omega_\Delta \subset \mathbb{R}_{\mathbf{x}}^d.$$

Here, $\mathbf{W}_\Delta = \{\mathbf{W}_{\mathbf{j}}\}$ is the computed *gridfunction* and $\mathbf{G}_{\mathbf{j}}$ are discrete approximations of the source term, $\mathbf{G}_{\mathbf{j}} \approx \mathbf{g}(\mathbf{x}_{\mathbf{j}})$. We can distinguish between two main classes of finite-difference methods:

(i) Boundary-value problems, such as (3.2), (3.3), (3.4), and (3.5), lead to nonlinear systems of algebraic equations, which we abbreviate

$$\text{(3.10a)} \qquad \qquad \mathbb{A}(\mathbf{W}_\Delta) = \mathbf{G}_\Delta.$$

The vector gridfunction $\mathbf{G}_\Delta$ accounts for the discrete source terms, $\{\mathbf{G_j}\}$, $\mathbf{x_j} \in \Omega_\Delta$, and the boundary data, $\{\mathbf{b_j}\}$, $\mathbf{x_j} \in \partial\Omega_\Delta$.

(ii) Time-dependent problems, such as (3.6), (3.7), (3.8), yield finite-difference schemes of the form

$$\text{(3.10b)} \qquad \qquad \mathbf{W}_\Delta^{n+1} = \mathbb{A}(\mathbf{W}_\Delta^n) + \Delta t \mathbf{G}_\Delta^n.$$

3.2. **Finite-element methods.** *Finite-element methods* (FEMs) offer great flexibility in modeling problems with complex geometries and, as such, they have been widely used in science and engineering as the solvers of choice for structural, mechanical, heat transfer, and fluid dynamics problems [190, 43, 114, 194, 44, 110, 25]. To this end, one partitions the domain of interest, $\Omega \subset \mathbb{R}_\mathbf{x}^d$, into a set of nonoverlapping polyhedrons, $\{T_j\}$. The grid, Ω_Δ, is a graph of such polyhedrons, $T_j \in \Omega$, and a set of their neighbors, T_{j_k}, $j_k \in \mathcal{N}(j)$, which form the *stencil* associated with T_j. The grid could be *structured*, e.g., a structured array of triangles derived from two-dimensional Cartesian rectangles, or it could be an *unstructured* grid of triangles or quadrilaterals in dimension $d = 2$, tetrahedra in $d = 3$, or other elements adapted to the underlying geometry of the PDE (2.1). Here, Δ abbreviates the diameter, $\Delta = \max_j \operatorname{diam}(T_j)$, such that the elements $|T_j|$ shrink uniformly as $\Delta \downarrow 0$. A finite-element approximation, $\mathbf{W}(\mathbf{x}) = \sum_j \mathbf{W}_j \varphi_j(\mathbf{x})$, is then realized in terms of piecewise polynomial *basis functions*, $\{\varphi_j\}$, where φ_j is a piecewise polynomial supported on the local stencil, $\{T_k\}_{k \in \mathcal{N}(j)}$, associated with T_j. Examples of two-dimensional triangular grids are depicted in Figure 3.5.

The platform of finite-element methods appeals to a wide range of nonlinear boundary-value PDEs, which are expressed in different formulations. We shall mention the main four.

(i) *Weak formulations.* As an example we begin with the weak formulation of the two-dimensional minimal surface equation (2.3) subject to homogeneous Dirichlet boundary conditions, which states that a solution w is sought such that for all $\varphi \in H_0^1(\Omega)$, there holds

$$\text{(3.11)} \qquad \mathcal{B}(w, \varphi) = \int_\Omega g(\mathbf{x})\varphi(\mathbf{x})d\mathbf{x}, \qquad \mathcal{B}(w, \varphi) := \int_\Omega \frac{\nabla_\mathbf{x} w \cdot \nabla_\mathbf{x} \varphi}{\sqrt{1 + |\nabla_\mathbf{x} w|^2}} d\mathbf{x}.$$
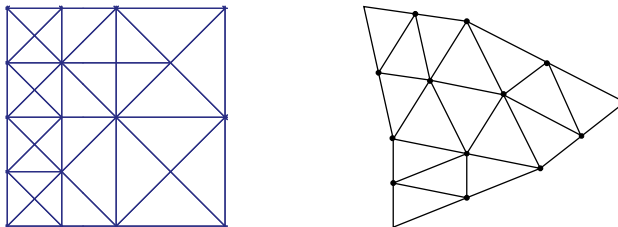

FIGURE 3.5. Structured and unstructured triangulation of two-dimensional domains.

To proceed with its FEM approximation, we partition Ω into a nonoverlapping triangulation $\Omega_\Delta := \{T_j\}$. A piecewise polynomial finite-element approximation is sought, $W(\mathbf{x}) = \sum_k W_k \phi_k(\mathbf{x})$, in terms of polynomial elements, $\varphi_k(\mathbf{x})$, supported on $\{T_\ell, \ell \in \mathcal{N}(k)\}$. This stencil of neighboring triangle elements emphasizes the local character of the FEM approximant. The integral representation of the minimal surface equation (3.11) is now tested against the subspace of all test functions, $\varphi \in \mathrm{span}\{\varphi_j\}$,

$$\mathcal{B}(W, \varphi_j) = \int_\Omega g(\mathbf{x})\varphi_j(\mathbf{x})d\mathbf{x}, \qquad \forall \varphi_j \in H_0^1(\Omega).$$

The computational versatility of FEMs is realized by decomposing the global problem (3.11) into simpler building blocks, which consist of polynomials over simple, Δ-small geometric elements. By assembling the contribution of the different triangular elements, we end up with a finite-element scheme,
(3.12a)

$$\sum_{k \in \mathcal{N}(j)} A_{jk}(W)W_k = G_j, \qquad G_j := \sum_{k \in \mathcal{N}(j)} \int_{T_k} g(\mathbf{x})\varphi_j(\mathbf{x})d\mathbf{x}, \qquad j = 1, 2, \ldots,$$

where $\{A_{jk}(W)\}$ is the *stiffness matrix*,

(3.12b) $$A_{jk}(W) = \int_{T_k} \frac{\nabla_{\mathbf{x}}\varphi_k \cdot \nabla_{\mathbf{x}}\varphi_j}{\sqrt{1 + |\sum_{\ell \in \mathcal{N}(k)} W_\ell \nabla_{\mathbf{x}}\varphi_\ell|^2}} d\mathbf{x}.$$

This amounts to a nonlinear system of algebraic equations, $\mathbb{A}(\mathbf{W}_\Delta) = G_\Delta$, relating the finite-element approximation, $\mathbf{W}_\Delta = \{W_k\}$, to the data, $G_\Delta = \{G_j\}$. The integrals on the right of (3.12b) are evaluated using exact quadratures. To this end, the polynomial element, $W(\mathbf{x})_{|T_j}$, is realized in terms of its pointvalues, W_{j_ℓ}, at preselected sets of nodes $\{\mathbf{x}_{j_\ell}\}_\ell$ scattered inside and along the boundary of T_j. By sharing common values of W_{j_ℓ}'s across boundaries of neighboring elements, FEMs enforce a minimal smoothness of their approximants while keeping the local nature of differentiation. The finite-element framework enables one to assemble, discretize, and derive an approximate FEM solution by solving the resulting large yet sparse systems of nonlinear algebraic equations (3.12) for the W_Δ's. The solution of such systems can be achieved by a host of direct of iterative methods. As we noted before in the context of finite-difference approximations, the solution strategy is often tied to the specific nature of the underlying PDEs; we mention in particular preconditioning techniques, conjugate gradient and multi-level methods [24, 92, 215, 216, 220, 179].

(ii) *Variational formulations.* Instead of a weak formulation one may appeal to a Dirichlet principle, a variational formulation where the solution of the (2.1) is sought as a minimizer of an appropriate "energy" functional [83, 76, 73, 191],

(3.13) $$\mathbf{w} = \arg\min_{\mathbf{u} \in \mathcal{W}} \mathcal{I}[\,\partial^{\mathbf{r}}\mathbf{u}, \partial^{\mathbf{r}-1}\mathbf{u}, \ldots, \mathbf{u}, \mathbf{x}\,].$$

Here, $\mathcal{W}$ is a properly defined class of functions adapted to the boundary (and other side) conditions attached to our problem, so that the PDE (2.1) is realized as the Euler–Lagrange equation associated with this energy functional. A discrete solution is now sought as the minimizer of (3.13) over the finite-element space, $\mathcal{W}_\Delta := \mathrm{span}\{\varphi_j\}_j \subset \mathcal{W}$, which in turn leads to a minimization algorithm for the unknowns, $\mathbf{W}_\Delta = \{\mathbf{W}_j\}$. This is the *Rayleigh–Ritz principle* which was the original

framework for the mathematical framework of FEMs [54]. Once again, the versatility of FEMs is realized here by decomposing the global problem (3.13) into simpler building blocks of polynomials supported over simple, Δ-small geometric elements. As an example, the variational formulation of the minimal surface equation, (2.3b), realized over a two-dimensional triangulation $\{T_j\}$ of a domain Ω, yields [115, 43]

$$W_\Delta = \underset{\{W_k\}}{\arg\min} \left\{ \sum_j \int_{T_j} \sqrt{1 + \Big| \sum_{k \in \mathcal{N}(j)} W_k \nabla_{\mathbf{x}} \varphi_k \Big|^2} d\mathbf{x} \; \Big| \; \sum_j W_j \varphi_j(\mathbf{x}) \right.$$
$$\left. \approx b(\mathbf{x}), \; \mathbf{x} \in \partial\Omega_\Delta \right\}.$$

The minimizers sought above can be found by standard iterative algorithms, such as conjugate gradient and Krylov-based methods [92].

(iii) *Saddle-point formulations.* As an example, we reformulate the minimal surface equation (2.3) as a first-order system for $\mathbf{w} = (\mathbf{u}, w)$, such that for all $\boldsymbol{\psi}, \nabla_{\mathbf{x}} \cdot \boldsymbol{\psi}, \varphi \in L^2(\Omega)$, there holds

$$\begin{cases} \int_\Omega (\sqrt{1 + |\nabla_{\mathbf{x}} w|^2} \, \mathbf{u} \cdot \boldsymbol{\psi} d\mathbf{x} + b(w, \boldsymbol{\psi}) = 0, \\[2mm] b(\varphi, \mathbf{u}) = \int_\Omega g(\mathbf{x}) \varphi(\mathbf{x}) d\mathbf{x}, \end{cases} \qquad b(p, \boldsymbol{\psi}) := \int_\Omega p \nabla_{\mathbf{x}} \cdot \boldsymbol{\psi} d\mathbf{x}.$$

Many problems encountered in applications can be decomposed into pairs, $\mathbf{w} = (\mathbf{u}, p)$ such that the solution $\mathbf{w}$ is sought a saddle-point of an appropriate functional $\mathcal{I}[\mathbf{u}, p]$. A canonical example is the pairing of stress and displacement in elasticity equations, e.g. [4, 27, 110]. The resulting saddle-point problems are solved using *mixed finite-element* methods [26, 9, 58, 4, 27], in which the basis functions $\boldsymbol{\psi}_j \in \boldsymbol{\Psi}_\Delta$ and $\varphi_j \in \Phi_\Delta$ are drawn from different but *compatible* discrete function spaces, $\boldsymbol{\Psi}_\Delta$ and Φ_Δ. After the assembly of the finite-elements, one ends with a nonlinear sparse system of algebraic equations, $\mathbb{A}(\mathbf{W}_\Delta) = G_\Delta$. The solution of such systems requires that we be careful: the saddle-point formulation renders a null block on the diagonal of $\mathbb{A}$ [4, 27]. As another example, we mention that the Monge–Ampère equation (2.5) can be reformulated as a saddle-point problem and its finite-element solution is sought using the *least squares method* [64, 23].

(iv) *Boundary-element methods.* Here one appeals to the *integral formulation* of elliptic problems. Nonlinear boundary-value PDEs which contain linear elliptic differential operators could be inverted in terms of Green's functions. One ends up with nonlinear singular integral formulation along the boundary of the domain. The works [113, 193] motivated a finite-element discretization of these Fredholm-type integral equations, which in turn led to the boundary-element method (BEM), [18, 17, 176, 62]. As before, one ends up with a nonlinear algebraic system of equations for the unknown boundary elements, $\{W_{\mathbf{j}}\}_{|\mathbf{x_j} \in \partial\Omega_\Delta}$. The global nature of the underlying integral equations renders a *full system* which is expensive to solve; the efficiency of the BEM is realized for problems where there is a small surface to volume ratio. Alternatively, one can accelerate the convergence by dedicated solvers, such as the *fast multipole method* [94], which yields a considerable speed-up in the solution of these full matrix equations.

We turn our attention to FEMs for time-dependent problems. A weak formulation of the one-dimensional convection-diffusion equation (2.7a) states that for all

$C_0^1(\mathbb{R})$-*test functions*, φ,

(3.14)
$$\frac{d}{dt} \int \mathbf{w}(t,x)\varphi(x)dx = \int \mathbf{F}(\mathbf{w}(t,x))\varphi'(x)dx$$
$$- \nu \int \mathbf{Q}(\partial_x \mathbf{w}(t,x))\varphi'(x)dx + \int \mathbf{g}(t,x)\varphi(x)dx.$$

We partition a given interval $\Omega \subset \mathbb{R}$ into a set of consecutive cells $\Omega_\Delta = \bigcup_k [x_k, x_{k+1})$, and we seek a piecewise *linear* FEM approximation, $\mathbf{W}(t,x) = \sum_k \mathbf{W}_k(t)\varphi_k(x)$, expressed in terms of the standard basis of piecewise linear "hat" functions,

$$\varphi_k(x) = \frac{x - x_{k-1}}{x_k - x_{k-1}}\mathbf{1}_{[x_{k-1},x_k)}(x) + \frac{x_{k+1} - x}{x_{k+1} - x_k}\mathbf{1}_{[x_k,x_{k+1})}(x), \qquad x_{k-1} \leq x \leq x_{k+1}.$$

The stencil associated with x_k occupies the neighboring gridpoints, $x_\ell, \ell \in \mathcal{N}(k) := \{k-1, k, k+1\}$. The discretization of the weak formulation (3.14) is now realized for the subspace of piecewise linear test functions, which is spanned by the φ_j's; setting $\varphi(x) = \varphi_j(x)$ in (3.14) yields

$$\sum_{k \in \mathcal{N}(j)} \left[\int \Big(\varphi_k(x), \varphi_j(x)\Big)dx \right] \frac{d}{dt}\mathbf{W}_k(t)$$
$$= \int \mathbf{F}\Big(\sum_{k \in \mathcal{N}(j)} \mathbf{W}_k(t)\varphi_k(x) \Big)\varphi_j'(x)dx$$
$$- \nu \int \mathbf{Q}\Big(\sum_{k \in \mathcal{N}(j)} \mathbf{W}_k(t)\varphi_k'(x) \Big)\varphi_j'(x)dx + \int \mathbf{g}(t,x)\varphi_j(x)dx.$$

Thus, the unknowns $\{\mathbf{W}_k\}$ are governed by the nonlinear system of ODEs
(3.15a)
$$\sum_{k \in \mathcal{N}(j)} M_{kj}\frac{d}{dt}\mathbf{W}_k(t) = -\Big(\mathbf{F}_{j+1/2} - \mathbf{F}_{j-1/2}\Big) + \nu\Big(\mathbf{Q}(D_+\mathbf{W}_j) - \mathbf{Q}(D_-\mathbf{W}_j)\Big) + \mathbf{G}_j(t).$$

On the left we have a tridiagonal invertible *mass matrix*,

$$M_{kj} := \int \varphi_j(x)\varphi_k(x)dx \approx \Delta x_j \delta_{jk}, \qquad \Delta x_j := \frac{x_{j+1} - x_{j-1}}{2};$$

on the right, $\mathbf{F}_{j+1/2}$ is the *numerical flux*,

(3.15b)
$$\mathbf{F}_{j+1/2} := \int_{\xi=0}^1 \mathbf{F}\Big(\xi\mathbf{W}_j + (1-\xi)\mathbf{W}_{j+1}\Big)d\xi.$$

We end up with a semidiscrete method of lines finite-element scheme for $\mathbf{W}_\Delta(t) := \{\mathbf{W}_k(t)\}$, which we abbreviate as

$$\frac{d}{dt}\mathbf{W}_\Delta = \mathbb{M}^{-1}\Big[-\mathbb{A}_\mathbf{F}(\mathbf{W}_\Delta) + \nu\mathbb{A}_\mathbf{Q}(\mathbf{W}_\Delta) \Big] + \mathbf{G}_\Delta(t), \qquad \mathbf{G}_\Delta := \{\mathbb{M}^{-1}\mathbf{G}_j(t)\}.$$

Numerical examples for the one-dimensional FEM (3.15) and the corresponding two-dimensional finite-element scheme [201] are shown in Figure 3.6.

The derivation of the finite-element schemes (3.12), (3.15) demonstrates several typical features of the general framework of FEM. Once the grid and the space of piecewise polynomials are chosen, then the weak formulation of the PDE dictates the final format of the finite-element scheme. In particular, the finite-element formulation *automatically* adapts itself to deal with general, unstructured grids: in (3.15), for example, the gridpoints need not be equispaced. We notice that in the
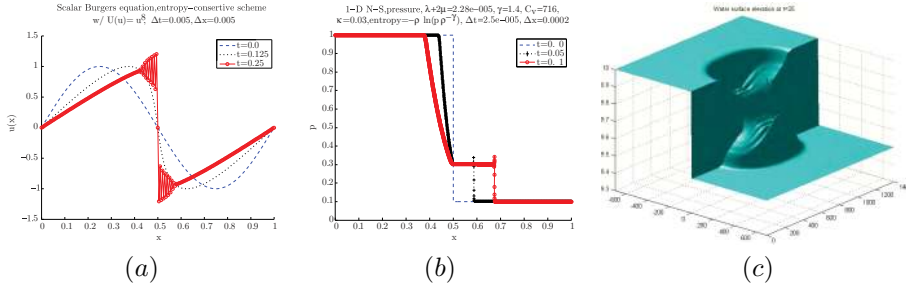
FIGURE 3.6. Computations using the one- and two-dimensional
finite-element scheme (3.15). (a) The inviscid Burgers equation,
(2.7b), $w_t + (w^2/2)_x = 0$. The dispersive character of the en-
tropy conservative scheme (3.15) yields the binary oscillations sur-
rounding the shock discontinuity [130]. (b) The time evolution of
a right moving pressure shock wave in one-dimensional Navier–
Stokes equations (2.7a) at $t = 0, t = 0.05$, and $t = 0.1$. (c) Water
surface elevation $h(x, y, t)$ in a dam-break problem modeled by the
irrotational shallow-water equations (2.8a) at $t = 25s$ [201].

simple case of piecewise linear elements, the computed FEM solution of (3.15) is
realized in terms of its pointvalues, $\mathbf{W}_j = \mathbf{W}(x_j)$. For more general polynomial-
based elements, the $\mathbf{W}_j$'s do not necessarily coincide with pointvalues but with
other local moments of the computed solution. There is a large catalog [5] of such
finite-element basis functions which provide approximations to any desired order.
The resulting FEM solution, $\mathbf{W}(\mathbf{x}) = \sum_j \mathbf{W}_j \varphi_j(\mathbf{x})$, is viewed as an approximant
throughout the computational domain. One should compare the FEM numerical
flux (3.15b) with the finite-difference flux (3.7),

$$\mathbf{F}_{j+1/2} = \frac{1}{2}(\mathbf{F}(\mathbf{W}_{j+1}) + \mathbf{F}(\mathbf{W}_j));$$

the latter depends only on the gridvalues $\mathbf{F}(\mathbf{W}_j), \mathbf{F}(\mathbf{W}_{j+1})$, whereas the former
involves all the intermediate values of $F(\cdot)$.

A rather general setup for the construction of finite-element schemes is offered by
the Galerkin formulation. To this end, we let Φ_Δ denote the finite-dimensional com-
putational space spanned by the finite-element basis functions, $\Phi_\Delta := \text{span}\{\varphi_j\}$.
In defining Φ_Δ, one has to specify three ingredients:

  (i) the partition, $\Omega_\Delta = \bigcup T_j$;
 (ii) the local basis functions, $\{\varphi_j\}$; and
(iii) the parameters to realize these local basis functions, e.g., using their point-
      values sampled at a preselected set of gridpoints.

The framework of finite-element methods offers a great variety of choices in each
one of these three ingredients. In particular, there are different methodologies for
the choice of basis functions, $\{\varphi_j\}$. We shall mention the most important three:

  (i) In "classical" FEMs, the φ_j's are polynomials of low degree with minimal
      requirement of continuity across the interfaces of the elements.

(ii) The FEM-based class of *hp-methods* [10] combine high-degree polynomials (of order p) with an increasing number of elements (of order h^{-d}, where h stands for the discretization parameter Δ).

(iii) On the other extreme, the class of *discontinuous Galerkin* methods uses basis functions which are allowed to experience jump discontinuities across the interfaces [173, 6]. These are particularly effective basis functions in problems with low regularity, such as the Eikonal equation [221] or problems with shock discontinuities [47, 142].

Let $\mathbb{P}_\Delta$ denote an appropriate *projection* into the computational space Φ_Δ. The *Galerkin method* for the PDE (2.1) seeks an approximate solution, $\mathbf{W} = \sum \mathbf{W}_j \varphi_j(\mathbf{x})$, such that

$$(3.16a) \qquad \mathbb{P}_\Delta \mathcal{A}(\partial^{\mathbf{s}} \mathbf{W}, \partial^{\mathbf{s}-1} \mathbf{W}, \ldots, \partial \mathbf{W}, \mathbf{W}, \mathbf{x}) = \mathbb{P}_\Delta \mathbf{g}(\mathbf{x}).$$

In the prototype case, the projection $\mathbb{P}_\Delta$ is induced by a weak formulation of (2.1) associated with an auxiliary *biform*, $\int_\Omega \mathcal{A}(\partial^{\mathbf{s}} \mathbf{w}, \ldots, \mathbf{w}, \mathbf{x}) \varphi(\mathbf{x}) \, d\mathbf{x} \to \mathcal{B}(\mathbf{w}, \boldsymbol{\varphi})$, such that (2.1), is recast into the form

$$\mathcal{B}(\mathbf{w}, \boldsymbol{\varphi}) = \int_\Omega g(\mathbf{x}) \boldsymbol{\varphi}(\mathbf{x}) d\mathbf{x}, \qquad \mathcal{B}(w, \boldsymbol{\varphi}) := \int_\Omega \mathcal{A}(\partial^{\mathbf{s}} \mathbf{w}, \ldots, \mathbf{w}, \mathbf{x}) \varphi(\mathbf{x}) \, d\mathbf{x}.$$

This is demonstrated with the example of the minimal surface equation (2.3a), which was recast into the weak formulation (3.11). The corresponding finite-element Galerkin approximation seeks $\mathbf{W} \in \Phi_\Delta$ such that for all test function φ_j,

$$(3.16b) \quad \mathcal{B}\Big(\sum_k \mathbf{W}_k \varphi_k, \varphi_j\Big) = \mathbf{G}_j, \qquad \mathbf{G}_j := \int \mathbf{g}(\mathbf{x}) \varphi_j(\mathbf{x}) d\mathbf{x}, \qquad j = 1, 2, \ldots.$$

By assembling the equations (3.16b) for $\mathbf{W}_\Delta = \{\mathbf{W}_k\}$, one ends up with a system of nonlinear algebraic equations, which we abbreviate as

$$(3.17a) \qquad\qquad \mathbb{A}(\mathbf{W}_\Delta) = \mathbf{G}_\Delta.$$

As before, $\mathbf{G}_\Delta$ accounts for the discrete source terms $\{\mathbf{G}_j\}$ and the boundary data, $\{\mathbf{b}_j\}$, $\mathbf{b}_j = \int_{\partial\Omega} \mathbf{b}(\mathbf{x}) \varphi_j(\mathbf{x}) d\mathbf{x}$. Similarly, the corresponding FEM for time-dependent problems reads

$$(3.17b) \qquad\qquad \mathbf{W}_\Delta^{n+1} = \mathbb{M}^{-1} \mathbb{A}(\mathbf{W}_\Delta^n) + \Delta t \mathbf{G}_\Delta^n.$$

Here, $\mathbb{M}$ is an invertible mass matrix, $\mathbb{M} = \{(\varphi_j, \varphi_k)\}$, $\mathbb{A}$ is the assembly of the nonlinear terms, $\mathbb{A}(\mathbf{W}_\Delta) = \Big\{ A\Big(\sum_k \mathbf{W}_k \varphi_k, \varphi_j \Big) \Big\}$, and $\mathbf{G}_\Delta^n = \{\mathbb{M}^{-1} \mathbf{G}^n\}$ captures the source and boundary terms. This is a generalization of the linear setup, in which case (3.17) is reduced to a linear system of equations, $\mathbb{A}(\mathbf{W}_\Delta) = \mathbb{A}\mathbf{W}_\Delta$, where $\mathbb{A}$ is the stiffness matrix, $\mathbb{A} := \{A(\varphi_k, \varphi_j)\}$.

3.3. **Finite-volume methods.** *Finite-volume* (FV) methods use the same grids as FEMs, by partitioning Ω into a set of (structured or unstructured) nonoverlapping polyhedral cells, $\Omega_\Delta = \{T_j\}$. FV schemes are realized in terms of *cell averages*, $\{\overline{\mathbf{W}}_j\}$, where one ends up with piecewise constant approximation, $\mathbf{W}(\mathbf{x}) = \sum_j \overline{\mathbf{W}}_j \mathbf{1}_{T_j}$. More general FV schemes employ higher-order local cell moments, which lead to higher-order piecewise polynomial approximations. Similar to finite-element methods, FV approximations are defined throughout the computational domain, and unlike finite-difference methods, they are not limited to discrete point-values. In contrast to FEMs, however, the FV approximations need not be smooth

across the edges of the cells. They are therefore suitable to simulate problems with large gradients and, in particular, the spontaneous formation of jump discontinuities in nonlinear conservation laws [89, 90, 49, 136, 197].

As a prototype example, we consider the one-dimensional inviscid convection equation (2.7b), whose solution is sought in terms of a piecewise linear FV approximation,

$$(3.18) \qquad \mathbf{W}(t^n, x) = \sum_j \left(\overline{\mathbf{W}}_j^n + (x - x_j)(\mathbf{W}')_j^n \right) \mathbf{1}_{I_j}(x).$$

Here, $I_j := [x_{j-1/2}, x_{j+1/2})$, are one-dimensional cells of fixed mesh size Δx, $\overline{\mathbf{W}}_j^n$ are the approximate cell averages, and $(\mathbf{W}')_j^n$ are the approximate first derivatives, which are related to the first-order local moments, $\int_{I_j} (x - x_j)\mathbf{W}(t^n, x)dx = (\Delta x)^3 (\mathbf{W}')_j^n / 12$. The globally defined FV solution $\mathbf{W}(t^n, x)$ evolves into an exact solution of (2.7b), $\mathbf{W}(t^n, x) \mapsto \mathbf{w}^n(t, x)_{|t > t^n}$,

$$(3.19) \quad t \geq t^n : \quad \partial_t \mathbf{w}^n(t, x) + \partial_x \mathbf{F}(\mathbf{w}^n(t, x)) = \mathbf{g}(t, x)$$
$$\text{subject to} \quad \mathbf{w}^n(t, x) = \mathbf{W}(t^n, x) \ \text{ at } \ t = t^n.$$

We realize this solution at $t^{n+1} = t^n + \Delta t$, in terms of its cell averages, $\overline{\mathbf{W}}_j^{n+1}$: integration of (3.19) over the *control volume* $I_j \times [t^n, t^{n+1})$ yields

$$(3.20a) \qquad \overline{\mathbf{W}}_j^{n+1} = \overline{\mathbf{W}}_j^n - \frac{\Delta t}{\Delta x} \left(\mathbf{F}_{j+\frac{1}{2}}^{n+\frac{1}{2}} - \mathbf{F}_{j-\frac{1}{2}}^{n+\frac{1}{2}} \right) + \Delta t \overline{\mathbf{G}}_j^{n+\frac{1}{2}}.$$

Here, $\overline{\mathbf{G}}_j^{n+\frac{1}{2}}$ is the approximate cell average of $\mathbf{g}(t, x)$ over $I_j \times [t^n, t^{n+1})$, and $\mathbf{F}_{j\pm\frac{1}{2}}^{n+\frac{1}{2}}$ are the *numerical fluxes*

$$(3.20b) \qquad \mathbf{F}_{j\pm\frac{1}{2}}^{n+\frac{1}{2}} = \frac{1}{\Delta t} \int_{t^n}^{t^{n+1}} \mathbf{F}\big(\mathbf{w}^n(\tau, x_{j\pm\frac{1}{2}})\big)d\tau.$$

To complete the formulation of the FV scheme (3.21), one needs to specify the missing approximate derivatives, $(\mathbf{W}')_j^n$. We shall mention three possible recipes for doing so.

(i) Set $(\mathbf{W}')_j^{n+1} \equiv 0$. This yields the celebrated Godunov scheme [89], the forerunner for all FV methods,

$$\overline{\mathbf{W}}_j^{n+1} = \overline{\mathbf{W}}_j^n - \frac{\Delta t}{\Delta x} \left(\mathbf{F}\big(\mathbf{w}_{j+\frac{1}{2}}^n\big) - \mathbf{F}\big(\mathbf{w}_{j-\frac{1}{2}}^n\big) \right) + \Delta t \overline{\mathbf{G}}_{j+1/2}^{n+\frac{1}{2}}.$$

Here, $\mathbf{w}_{j+\frac{1}{2}}^n = \mathbf{w}^n(t^{n+\frac{1}{2}}, x_{j+\frac{1}{2}})$ is the solution of a (generalized) Riemann problem (3.19) localized along the interface $\{(\tau, x_{j+\frac{1}{2}}) : t^n < \tau \leq t^{n+1}\}$. The initial discontinuities at the initial stage of these interfaces, $(t^n, x_{j\pm\frac{1}{2}})$ are resolved into nonlinear waves and a proper *Riemann solver* is required to accumulate those waves, which impinge on the interfaces at $t = t^{n+\frac{1}{2}}$ from within the cell I_j [177, 212]. To this end, one needs to trace left-going and right-going waves, which is the hallmark of so-called *upwind schemes.*

(ii) To gain additional resolution, one may consider a second approach of *reconstructing* the missing numerical derivatives, $(\mathbf{W}')_j^n$, from the computed cell averages, $\{\overline{\mathbf{W}}_j^n\}$. For example, one may use a (possibly nonlinear) combination of
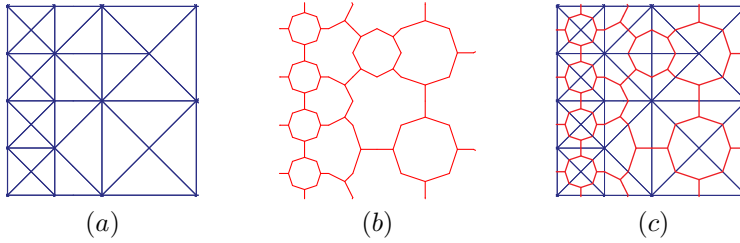
FIGURE 3.7. (a) A triangular grid, (b) a dual grid, and (c) the resulting staggered grid [127]

forward and backward differences

$$(3.20c) \qquad (\mathbf{W}')_j^n = \mathcal{S}\Big(\dots, D_\pm \overline{\mathbf{W}}_{j+1}^n, D_+ \overline{\mathbf{W}}_j^n, D_- \overline{\mathbf{W}}_j^n, D_\pm \overline{\mathbf{W}}_{j-1}^n, \dots, \Big).$$

There is a whole library of such modern recipes (called *limiters*), which enable one to reconstruct $\mathbf{W}(t^n, x)$ from its cell averages in the "direction of smoothness", while preserving the nonoscillatory behavior of the underlying exact solution $\mathbf{w}^n(t, x)$. The intense period of development of such limiters during the 1980s and 1990s was marked by a series of acronyms such as the second-order MUSCL and TVD scheme [135, 100, 192], cubic-order PPM scheme [50], and the class of higher-order (W)ENO schemes [102, 101, 186, 141, 49, 79].

(iii) A third approach is to *evolve* the missing numerical derivatives, $(\mathbf{W}')_j^n$, using, e.g., a *discontinuous Galerkin method* [47, 142]. Here, FV methods meet FEM, (3.17b), with evolved basis functions $\varphi_j(x) = \big(\overline{\mathbf{W}}_j^n + (x - x_j)(\mathbf{W}')_j^n\big)\mathbf{1}_{I_j}(x)$.

In summary, starting with the FV representation (3.18), and followed by the various steps of (3.20), one ends up with the general class of upwind FV schemes,

$$\mathbf{W}(t^n, x) \mapsto \sum_j \big(\overline{\mathbf{W}}_j^{n+1} + (x - x_j)(\mathbf{W}')_j^{n+1}\big)\mathbf{1}_{I_j}(x).$$

To avoid the intricate and time-consuming Riemann solvers for upwind FV schemes, another class of *central* FV schemes was developed, which employ the FV representation over *staggered grids*. Examples of such two-dimensional staggered grids are depicted in Figure 3.7.

We demonstrate the one-dimensional framework of such central schemes in the context of the same inviscid convection equation we had before (2.7b), whose solution is sought in terms of a piecewise linear FV approximation,

$$\mathbf{W}(t^n, x) = \sum_j \Big(\overline{\mathbf{W}}_j^n + (x - x_j)(\mathbf{W}')_j^n\Big)\mathbf{1}_{I_j}(x).$$

To avoid the discontinuous edges at $x_{j\pm1/2}$, however, one computes the FV solution at $t^{n+1} = t^n + \Delta t$ over the *staggered grid*, $I_{j+1/2}$: integration of the PDE (2.7b) over the control volumes $I_{j+1/2} \times [t^n, t^{n+1})$ yields

$$(3.21a) \qquad \begin{aligned} \overline{\mathbf{W}}_{j+1/2}^{n+1} =& \frac{1}{2}\big(\overline{\mathbf{W}}_j^n + \overline{\mathbf{W}}_{j+1}^n\big) + \frac{\Delta x}{8}\Big((\mathbf{W}')_j^n - (\mathbf{W}')_{j+1}^n\Big) \\ & - \frac{\Delta t}{\Delta x}\Big(\mathbf{F}_{j+1}^{n+\frac{1}{2}} - \mathbf{F}_j^{n+\frac{1}{2}}\Big) + \Delta t\,\overline{\mathbf{G}}_{j+1/2}^{n+\frac{1}{2}}. \end{aligned}$$

Here, $\overline{\mathbf{G}}_{j+1/2}^{n+\frac{1}{2}}$ is the approximate cell average of $\mathbf{g}(t,x)$ over $I_{j+1/2} \times [t^n, t^{n+1})$ and $\mathbf{F}_j^{n+\frac{1}{2}}$ are the numerical fluxes evaluated at the intermediate pointvalues, $\mathbf{W}_j^{n+1/2}$,
(3.21b)
$$\mathbf{F}_j^{n+\frac{1}{2}} = \mathbf{F}(\overline{\mathbf{W}}_j^{n+\frac{1}{2}}), \qquad \mathbf{W}_j^{n+\frac{1}{2}} := \overline{\mathbf{W}}_j^n - \frac{\Delta t}{2}\left(\mathbf{F}_{\mathbf{W}}(\overline{\mathbf{W}}_j^n)(\mathbf{W}')_j^n + \mathbf{g}(t^n, \mathbf{x}_j)\right).$$

As before, one needs to specify the missing approximate derivatives, $(\mathbf{W}')_j^n$, and we mention three possible recipes for doing so.

(i) Set $(\mathbf{W}')_j^n \equiv 0$. This yields the Lax–Friedrichs scheme [128], the forerunner for all central schemes,
$$\overline{\mathbf{W}}_{j+1/2}^{n+1} = \overline{\mathbf{W}}_{j+1/2}^n - \frac{\Delta t}{\Delta x}\left(\mathbf{F}(\overline{\mathbf{W}}_{j+1}^n) - \mathbf{F}(\overline{\mathbf{W}}_j^n)\right)$$
$$+ \frac{1}{2}\left(\overline{\mathbf{W}}_j^n - 2\overline{\mathbf{W}}_{j+1/2}^n + \overline{\mathbf{W}}_{j+1}^n\right) + \Delta t \overline{\mathbf{G}}_{j+1/2}^{n+\frac{1}{2}}.$$

Here, FV methods meet finite difference methods, (3.10b), when the cell averages $\overline{W}_j^n$ are viewed as the gridvalues W_j^n. The expression inside the last parenthesis on the right,

(3.21c) $$\frac{1}{2}\left(\overline{\mathbf{W}}_j^n - 2\overline{\mathbf{W}}_{j+1/2}^n + \overline{\mathbf{W}}_{j+1}^n\right) \approx \frac{(\Delta x)^2}{4\Delta t}\partial_x^2 \overline{\mathbf{W}}(t^n, x_j),$$

is an example of a second-order *numerical dissipation* [122]. This excessive dissipation of vanishing order $(\Delta x)^2/\Delta t \to 0$ comes at the expense of lost resolution.

(ii) To gain additional resolution, one can use nonoscillatory reconstruction of the missing numerical derivatives from the computed cell averages, yielding the Nessyahu–Tadmor scheme and its extensions [155, 126]:

(3.21d) $$(\mathbf{W}')_j^n = \mathcal{S}\left(\ldots, D_+\overline{\mathbf{W}}_j^n, D_-\overline{\mathbf{W}}_j^n, \ldots\right).$$

Here, $\mathcal{S}$ stands for any limiter from the library of MUSCL, TVD, PPM, (W)ENO limiters.

(iii) Finally, a third possible approach for specifying the missing approximate derivatives, $(\mathbf{W}')_j^n$, is to *evolve* these missing numerical derivatives, using, e.g., a *discontinuous Galerkin method* [47, 142].

In summary, starting with the FV representation (3.18) and followed by the various steps of (3.21), one ends up with the general class of central FV schemes, which alternate between two dual grids,
$$\mathbf{W}(t^n, x) \mapsto \sum_j \left(\overline{\mathbf{W}}_{j+\frac{1}{2}}^{n+1} + (x - x_{j+\frac{1}{2}})(\mathbf{W}')_{j+\frac{1}{2}}^{n+1}\right)\mathbf{1}_{I_{j+\frac{1}{2}}}(x).$$

Figure 3.8 demonstrates three different examples of numerical simulation of sharp gradients using FV central schemes (3.21)

We turn to the multidimensional framework. As an example, we consider a weak formulation of the two-dimensional chemotaxis model (2.9), which is formulated on a triangular grid, $\Omega = \bigcup_j T_j$,

(3.22) $\dfrac{d}{dt}\displaystyle\int_{T_j} w(t, \mathbf{x})d\mathbf{x} = \kappa \int_{\partial T_j} \mathbf{n}(\mathbf{x})\cdot\nabla_{\mathbf{x}}c(t, \mathbf{x})w(t, \mathbf{x})d\mathbf{x} + \int_{\partial T_j} \mathbf{n}(\mathbf{x})\cdot\nabla_{\mathbf{x}}w(t, \mathbf{x})d\mathbf{x}.$

Here $\mathbf{n}(\mathbf{x})$ is the outward normal along the boundary of T_j. The FV method seeks a piecewise constant approximation of the density $w(t, \mathbf{x})$, $W(t, \mathbf{x}) = \sum_j \overline{W}_j(t)\mathbf{1}_j(\mathbf{x})$, and a piecewise-linear representation for the approximate concentration, $C(t, \mathbf{x}) =$
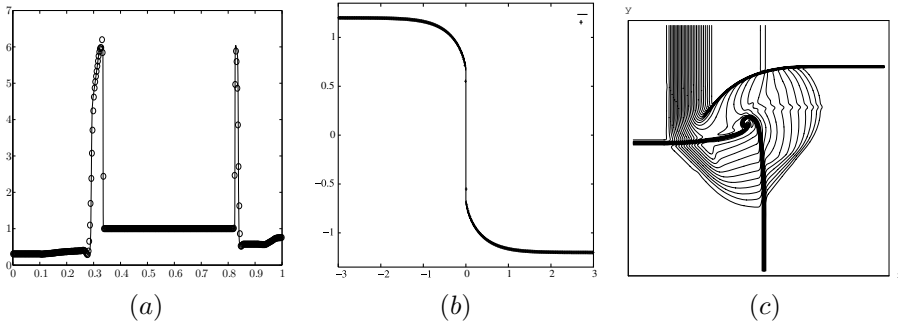
FIGURE 3.8. Numerical solution using FV central schemes. (a) Density of compressible Euler equations computed at $t = 0.01$ using a central discontinuous Galerkin method [142]. (b) Saturating dissipation, $w_t + f(w)_x = \left(w_x/\sqrt{1 + w_x^2}\right)_x$ [126]. (c) Density contours of two-dimensional Riemann problem (without a Riemann solver).

$\sum_k C_k(t)\varphi_k(\mathbf{x})$. The boundary integrals on the right of (3.22) are evaluated by approximate quadratures, based on boundary gridvalues, $w(t, \mathbf{x}_{j_\ell})$ and $\nabla_{\mathbf{x}}c(t, \mathbf{x}_{j_\ell})$. To this end, one employs *numerical fluxes* to reconstruct approximate boundary values by a judicious nonlinear combination of the neighboring cell averages and concentration values $\{\overline{W}_k, C_k \mid k \in \mathcal{N}(j)\}$. For example, the first integral on the right of (3.22), involving the differential flux, $\mathbf{F}(c, w) := \nabla_{\mathbf{x}}c(t, \mathbf{x})w(t, \mathbf{x})$, is approximated by

$$\int_{\partial T_j} \mathbf{n}(\mathbf{x}) \cdot \nabla_{\mathbf{x}}c(t, \mathbf{x})w(t, \mathbf{x}) \approx \sum_\ell \omega_\ell \, \mathbf{n}(\mathbf{x}_{j_\ell}) \cdot \mathbf{F}_{j_\ell}\left\{C_{k \in \mathcal{N}(j)}(t), \overline{W}_{k \in \mathcal{N}(j)}(t)\right\},$$

where ω_ℓ are the proper weights for the quadrature rule on the right. The resulting FV approximation of (2.9) amounts to a *semidiscrete* system of nonlinear ODEs for the cell averages

(3.23a)
$$\begin{aligned}
\frac{d}{dt}\overline{W}_j(t) = {} & \kappa \sum_\ell \omega_\ell \, \mathbf{n}(\mathbf{x}_{j_\ell}) \cdot \mathbf{F}_{j_\ell}\left\{C_{k \in \mathcal{N}(j)}(t), \overline{W}_{k \in \mathcal{N}(j)}(t)\right\} \\
& + \sum_\ell \omega_\ell \, \mathbf{n}(\mathbf{x}_{j_\ell}) \cdot \mathbf{Q}_{j_\ell}\left\{\overline{W}_{k \in \mathcal{N}(j)}(t)\right\}.
\end{aligned}$$

Here, $\mathbf{F}_{j_\ell}\{\cdot, \cdot\}$ and $\mathbf{Q}_{j_\ell}\{\cdot\}$ are the convective and diffusive numerical fluxes, respectively, depending on the concentrations $\{C_k\}$, which in turn are determined as the FEM solution of the Poisson equation (2.9b):

(3.23b) $$\sum_{k \in \mathcal{N}(j)} C_k(t) \int_{x \in T_k} \nabla\varphi_k(\mathbf{x}) \cdot \nabla\varphi_j(\mathbf{x})d\mathbf{x} = \sum_{k \in \mathcal{N}(j)} \overline{W}_k(t) \int_{x \in T_k} \varphi_j(\mathbf{x}).$$

A numerical example for an FV computation of the chemotaxis model (2.9) is provided in Figure 3.9.

FV methods for elliptic and parabolic equations were introduced in [211, 180, 181]. For recent progress in this direction, we refer to [45, 77] and the references therein. As with the FEM framework, one ends up with nonlinear system of algebraic equations for the FV solution which is realized in terms of few local moments,
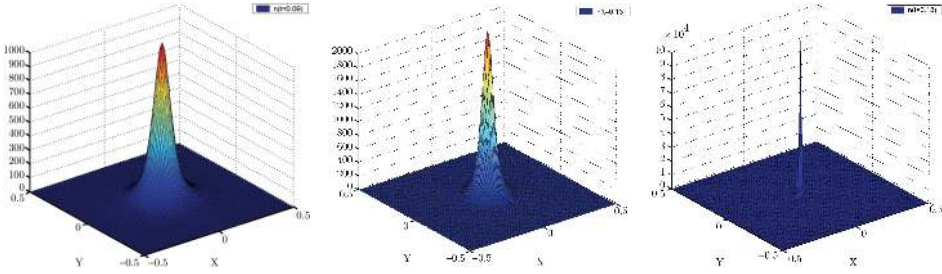
FIGURE 3.9. A finite-volume simulation [78] for the blow-up of Patlak–Keller–Segel chemotaxis model (2.9) at $t = 0.09, t = 0.13$, and $t = 0.18$.

$$\mathbf{W}_\Delta = \{\overline{\mathbf{W}}_j, \mathbf{W}'_j, \mathbf{W}''_j, \ldots, \}$$

$$(3.24a) \qquad\qquad\qquad \mathbb{A}(\mathbf{W}_\Delta) = \mathbf{G}_\Delta.$$

Similarly, the corresponding FV schemes for time-dependent problems read

$$(3.24b) \qquad\qquad \mathbf{W}_\Delta^{n+1} = \mathbb{M}^{-1}\mathbb{A}(\mathbf{W}_\Delta^n) + \Delta t \mathbf{G}_\Delta^n.$$

A main feature of FV schemes is the reconstruction of approximate *pointvalues* along the cell's boundaries, $\{\mathbf{W}(t^{n+\frac{1}{2}}, \mathbf{x}) \mid \mathbf{x} \in \partial T_j\}$, which are recovered from the computed local moments, $\mathbf{W}_\Delta = \{\overline{\mathbf{W}}_j, \mathbf{W}'_j, \mathbf{W}''_j, \ldots\}$. This led to the development of essentially nonlinear FV schemes, in the sense that their upwind or central stencils are data dependent.

3.4. **Spectral methods.** *Spectral methods* employ *spectral representations* of approximate solutions for nonlinear PDEs (2.1), $\mathbf{W}(\mathbf{x}) = \sum_{\mathbf{k}} \widehat{\mathbf{W}}_{\mathbf{k}}\varphi_{\mathbf{k}}(\mathbf{x})$. The local character of the building blocks in finite-difference, finite-element and finite-volume methods is lost. Instead, the basis functions of spectral methods are determined by discrete *orthogonality* with respect to preselected sets of collocation gridpoints, $\{\mathbf{x}_{\mathbf{j}}\}$. This leads to *global interpolants* with one-to-one correspondence between the spectral data $\{\widehat{\mathbf{W}}_{\mathbf{k}}\}$ and the *pointvalues*, $\{\mathbf{W}_{\mathbf{j}} = \mathbf{W}(\mathbf{x}_{\mathbf{j}})\}$.

We begin with a time-dependent periodic problem [159, 123, 93, 19, 103]. As an example, we consider the Schrödinger equation (2.6) over a 2π-torus, $\Omega = \mathbb{T}^d_{\mathbf{x}}$, which is covered by a Cartesian grid of $(2N + 1)^d$ equispaced gridpoints:

$$\mathbf{x}_{\mathbf{j}} = (j_1\Delta x_1, \ldots, j_d\Delta x_d), \qquad \mathbf{j} := (j_1, \ldots, j_d) \in \mathbb{Z}^d, \qquad \mathbf{\Delta x} := (\Delta x_1, \ldots, \Delta x_d),$$
$$- N \le j_\ell \le N.$$

An approximate solution of the periodic Schrödinger equation, $\mathbf{W}_N(t, \mathbf{x})$, is sought in terms of the discrete Fourier coefficients, $\widehat{\mathbf{W}}_{\mathbf{k}}$,

$$\mathbf{W}_N(t, \mathbf{x}) = \sum_{|k_\ell| \le N} \widehat{\mathbf{W}}_{\mathbf{k}}(t)e^{i\mathbf{k}\cdot\mathbf{x}}, \quad \widehat{\mathbf{W}}_{\mathbf{k}}(t) := \sum_{|j_\ell| \le N} \mathbf{W}(t, \mathbf{x}_{\mathbf{j}})e^{-i\mathbf{j}\cdot\mathbf{x}_k}\langle\mathbf{\Delta x}\rangle,$$
$$\mathbf{k} = (k_1, \ldots, k_d) \in \mathbb{Z}^d,$$

where $\langle\mathbf{\Delta x}\rangle$ is the volume of the d-dimensional cell $\langle\mathbf{\Delta x}\rangle := \prod_{j=1}^d \frac{\Delta x_j}{2\pi}$. Observe that differentiation can be carried out *exactly* as an algebraic operation in Fourier

space,

$$\partial_{\mathbf{x}}^{\mathbf{s}}\mathbf{W}_N(t,\mathbf{x}) = \sum_{|k_\ell|\leq N}(ik_1)^{s_1}\cdots(ik_d)^{s_d}\widehat{\mathbf{W}}_{\mathbf{k}}(t)e^{i\mathbf{k}\cdot\mathbf{x}}, \qquad \mathbf{s} = (s_1,\ldots,s_d) \in \mathbb{Z}_+^d.$$

The discrete Fourier coefficients, $\widehat{\mathbf{W}}_{\mathbf{k}}$, are accessible via the fast Fourier transform (FFT) [52]. To derive a spectral approximation of (2.6), we use its *discrete* weak formulation:

(3.25)

$$i\hbar\frac{d}{dt}\sum_{\mathbf{j}}\mathbf{w}(t,\mathbf{x_j})\varphi(\mathbf{x_j})\langle\Delta\mathbf{x}\rangle$$

$$= -\frac{\hbar^2}{2m}\sum_{\mathbf{j}}\Delta_{\mathbf{x}}\mathbf{w}(t,\mathbf{x_j})\cdot\varphi(\mathbf{x_j})\langle\Delta\mathbf{x}\rangle + \sum_{\mathbf{j}}V\big(\mathbf{w}(t,\mathbf{x_j})\big)\mathbf{w}(t,\mathbf{x_j})\varphi(\mathbf{x_j})\langle\Delta\mathbf{x}\rangle.$$

An approximation to the exact solution, $\mathbf{w}(t,\mathbf{x}) = \sum_{|\mathbf{k}|\leq\infty}\widehat{\mathbf{w}}_{\mathbf{k}}(t)e^{i\mathbf{k}\cdot\mathbf{x}}$, is sought in terms of a trigonometric polynomial, $\mathbf{W}_N(t,\mathbf{x})$. To this end, we use the orthogonal set of trigonometric test functions, $\Phi_N = \text{span}\{\varphi_{\mathbf{j}} = e^{i\mathbf{j}\cdot\mathbf{x}}\}_{|j_\ell|\leq N}$. We now use $\varphi \in \Phi_N$ as the test functions in (3.25): since by orthogonality, $\sum_{\mathbf{k}}\varphi_{\mathbf{p}}(\mathbf{x_k})\varphi_{\mathbf{q}}(\mathbf{x_k})\langle\Delta\mathbf{x}\rangle = \delta_{\mathbf{pq}}$, we end up with the spectral scheme for $\mathbf{W_j} \equiv \mathbf{W_j}(t)$,

(3.26) $\quad i\hbar\dfrac{d}{dt}\mathbf{W_j} = -\dfrac{\hbar^2}{2m}\Delta_{\mathbf{x}}\mathbf{W_j} + V\left(\mathbf{W_j}\right)\mathbf{W_j}, \qquad \Delta_{\mathbf{x}}\mathbf{W_j} := -\sum_{|k_\ell|\leq N}|\mathbf{k}|^2\widehat{\mathbf{W}}_{\mathbf{k}}e^{i\mathbf{k}\cdot\mathbf{x_j}}.$

This amounts to a semidiscrete (method of lines) system of nonlinear ODEs for the pointvalues $\{\mathbf{W_j}(t)\}$. The spectral scheme (3.26) furnishes an exact statement of Schrödinger equation (2.6) at the collocation points, $\mathbf{x_j}$. Observe that the computation of the Laplacian, $\Delta_{\mathbf{x}}\mathbf{W_j} = -\sum_{|k_\ell|\leq N}|\mathbf{k}|^2\widehat{\mathbf{W}}_{\mathbf{k}}e^{i\mathbf{k}\cdot\mathbf{x_j}}$, is carried out in the

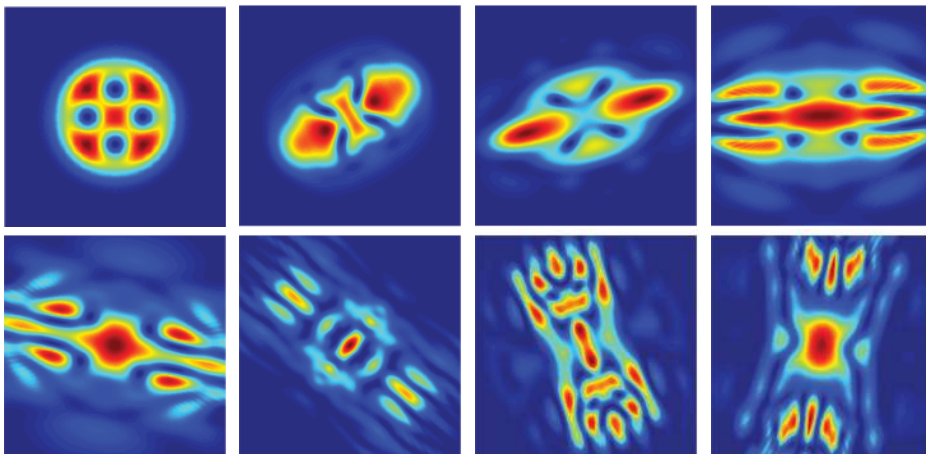FIGURE 3.10. Contour plots of the density, $|\mathbf{w}(\mathbf{x},t)|^2$, using a pseudo-spectral computation [13], for the interaction of two vortex dipoles in a rotating two-dimensional Bose–Einstein condensate governed by the Schrödinger equation (2.6) with potential $V = V(\mathbf{x},\partial,\mathbf{w}) = |\mathbf{x}|^2 + i\partial_\theta + 200|\mathbf{w}|^2$.

Fourier space, and in contrast to finite-difference, finite-element, and finite-volume methods, spectral approximations of differential operators such as the Laplacian, are *exact* for all the Fourier modes, $|\mathbf{k}_\ell| \leq N$. Algebraic operations, however, such as composition of $V(\mathbf{W})$ or multiplication, $V(\mathbf{W})\mathbf{W}$, are carried out as *exact* operations over the computational grid $\{\mathbf{x}_j\}$. A numerical example for spectral Fourier computation of the Schrödinger equation (2.6) is provided in Figure 3.10.

As our next example for spectral methods we consider the quasilinear system of inviscid convection equations (2.7b) over the interval $\Omega = [-1, 1]$. Its discrete weak formulation, corresponding to (3.14) with $\nu = 0$, reads

$$(3.27) \quad \frac{d}{dt} \sum_j \mathbf{w}(t, x_j)\varphi(x_j)\omega_j = \sum_j \mathbf{F}(\mathbf{w}(t, x_j))\varphi'(x_j)\omega_j + \sum_j \mathbf{g}(t, x_j)\varphi(x_j)\omega_j,$$

$$\forall \varphi \in C_0^1[-1, 1].$$

Here, the x_j's and ω_j's are the collocation points and the weights, respectively, which retain the exactness of certain Gauss quadratures with the corresponding integrals in (3.14). Since the problem is nonperiodic, the discrete equations (3.27) are augmented with appropriate Dirichlet- or Neumann-type boundary conditions at $x = \pm 1$. We now seek a spectral approximant in terms of *algebraic polynomials* [93, 214]. We proceed by expressing the spectral approximant in terms of the orthogonal family of *Legendre polynomials*, $\{p_k(x)\}_{k \geq 0}$:

$$\mathbf{W}_N(t, x) = \sum_{k=0}^{N} \widehat{\mathbf{W}}_k(t) p_k(x), \qquad \widehat{\mathbf{W}}_k(t) = \sum_{j=0}^{N} \mathbf{W}(t, x_j) p_k(x_j)\omega_j.$$

Observe that the approximant $\mathbf{W}_N(t, x)$ can be realized in one of two equivalent ways: either as the interpolant of the pointvalues, $\{\mathbf{W}_j(t) = \mathbf{W}(t, x_j)\}_{j=0}^{N}$, where the Gauss collocation points, $-1 = x_0 < x_1 \cdots < x_N = 1$, are chosen as the N zeroes of $(1 - x^2)p'_N(x)$; or in the dual space in terms of the discrete Legendre coefficients, $\{\widehat{\mathbf{W}}_k(t)\}_{k=0}^{N}$. We substitute the Nth degree spectral approximant, $\mathbf{W}_N(t, \mathbf{x})$, for the exact solution $\mathbf{w}(t, x) = \sum_{k \leq \infty} \widehat{\mathbf{w}}_k(t) p_k(x)$, and we use the polynomial N-space, $\Phi_N = \text{span}\{p_k\}_{k \leq N}$, as the test space for (3.27). To this end, we test (3.27) with the Nth degree polynomial test functions, $\varphi \in \text{span}\{\varphi_k(x)\}_{k=0}^{N}$, where $\varphi_k(x_j) = \delta_{jk}$. We end up with the *Legendre spectral scheme*,

$$(3.28a) \quad \frac{d}{dt}\mathbf{W}_N(t, x_j) + \partial_x \mathbf{F}(\mathbf{W}_N(t, x_j)) = \mathbf{SV}_N(\mathbf{W}_N(t, x_j)) + \mathbf{g}(t, x_j),$$

$$j = 1, 2, \ldots, N - 1.$$

As before, algebraic operations are carried out in physical space and differential operations are carried out in the spectral space of Legendre polynomials. Thus, for example, on the left of (3.28a) we compute the exact derivative of the numerical flux in terms of the derivatives of $\{p_k(x)\}$ at the computational gridpoints, $\{x_j\}$,

$$(3.28b) \quad \begin{aligned} \partial_x \mathbf{F}(\mathbf{W}_N(t, x_j)) &= \sum_{k=0}^{N} \widehat{\mathbf{F}(\mathbf{W})}_k(t) p'_k(x_j), \\ \widehat{\mathbf{F}(\mathbf{W})}_k(t) &= \sum_{j=0}^{N} \mathbf{F}(\mathbf{W}(t, x_j)) p_k(x_j)\omega_j. \end{aligned}$$
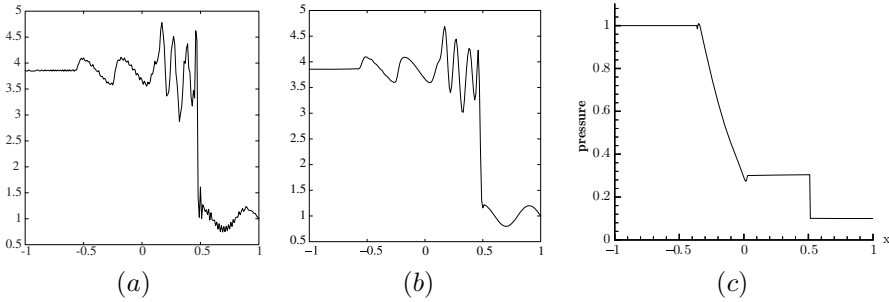
FIGURE 3.11. Computations using the Legendre spectral viscosity scheme (3.28). (a) A density field in Euler equations, (2.7a), using $N = 220$ modes. (b) The density field after postprocessing. (c) the pressure field after postprocessing (compare with the FEM solution in Figure 3.6(b)).

To complete the description of the Legendre spectral scheme, one may need to augment (3.28b) with appropriate boundary conditions of $\mathbf{W}_N(t, \pm 1)$. On the right of (3.28a) we have added a judicious amount of so-called *spectral viscosity*:

$$(3.28c) \qquad \mathbf{SV}_N\big(\mathbf{W}_N(t, x_j)\big) := -N \sum_{k=0}^{N} \left(\frac{k}{N}\right)^{2\sigma} \widehat{\mathbf{W}}_k(t) p_k(x_j), \qquad \sigma \gg 1.$$

Without it, the spectral solution may develop spurious Gibbs oscillations [195]. Observe that the spectral viscosity term in (3.28c) adds a negligible amount of numerical dissipation for low modes, $k \ll N$, when compared, for example, with the numerical dissipation in the FV scheme (3.21c). Figure 3.11(a) demonstrates the solution of the Euler equations (2.7b) using Legendre spectral viscosity [195, 197]. When the underlying solutions contain large gradients, such as shock discontinuities depicted in the density in Figure 3.11(a), spectral representations suffer from spurious Gibbs oscillations. To this end, one needs to *postprocess* the computed spectral solution [143, 151, 199]. The preprocessed Gibbs oscillations and postprocessed spectral results are depicted in Figure 3.11(b)–(c).

In a similar manner, other families of orthogonal polynomials lead to the Chebyshev spectral method, Hermite spectral method, etc.

The derivation of the spectral schemes (3.26), (3.28) demonstrates several typical features of spectral methods. In particular, the use of basis functions which are globally supported over the whole domain Ω, leads to spectral stencils which are global, in contrast to the local stencils of finite-difference, finite-element, and finite-volume methods. Moreover, spectral methods are "tied" to Cartesian geometries and preselected sets of collocation points to realize these global basis functions. Despite the availability of fast transform methods, the implementation of spectral schemes is therefore computationally intensive, due to the fact that there are $\sim N^d$ gridpoints. The main advantage of spectral methods, however, is their high resolution, which requires much smaller N's to achieve the same resolution as local methods based on a discretization parameter Δ. The efficiency of spectral vs. other methods in this context of high resolution can be quantified in terms of the saving in the number of degrees of freedom involved, $N^d \ll |\Omega|/\Delta^d$. Convincing evidence

is provided by the success of spectral methods in numerical weather prediction [174, 38, 116].

We turn our attention to boundary-value problems. The global character of spectral representations leads to major difficulties in their implementation for such problems, where one ends up with nonlinear algebraic systems which are *dense*: the computed pointvalues, $\{\mathbf{W}_N(\mathbf{x_j})\}$, are all connected throughout the computational domain. There are several ways to avoid such prohibitively expensive computation. We mention in this context the important **spectral element methods** [162, 20, 103]. Spectral element methods implement spectral representations on subdomains, $\Omega = \bigcup_j \Omega_j$, which are augmented with compatible boundary conditions at the interfaces, along $\partial \Omega_j$. In this fashion, one combines the local nature and geometric flexibility of FEMs with the high resolution of spectral methods (indeed, these methods can be viewed as the limiting case of the FEM-based hp-methods with $p = \infty$). The resulting algebraic systems amount to matrices with sparse blocks, which reflect the semilocal nature of the spectral element methods.

A general description of spectral methods is offered by the Galerkin formulation (3.16a),

$$\mathbb{P}_N \mathcal{A}(\partial^{\mathbf{s}}\mathbf{W}_N, \partial^{\mathbf{s}-1}\mathbf{W}_N, \dots, \partial\mathbf{W}, \mathbf{W}, \mathbf{x}) = \mathbb{P}_N \mathbf{g}(\mathbf{x}).$$

Here, $\mathbb{P}_N$ is a projection to the computational N-space, $\Phi_N = \mathrm{span}\{\varphi_{\mathbf{j}}\}$, spanned by orthogonal basis functions of trigonometric or algebraic polynomials of degree $|\mathbf{j}| \leq N$.

Spectral schemes can be realized either in terms of their pointvalues, $\mathbf{W}_\Delta = \{\mathbf{W}_N(x_{\mathbf{j}})\}$, or in terms of the coefficients, $\mathbf{W}_\Delta = \{\widehat{\mathbf{W}}_{\mathbf{k}}\}$. We end up with the nonlinear system of algebraic equations

$$(3.29a) \qquad\qquad\qquad \mathbb{A}(\mathbf{W}_\Delta) = \mathbf{G}_\Delta.$$

Similarly, we have spectral schemes for time-dependent problems. Expressed either in terms of the pointvalues, $\mathbf{W}_\Delta^n := \{\mathbf{W}(t^n, \mathbf{x_j})\}$, or their spectral coefficients, $\mathbf{W}_\Delta^n = \{\widehat{\mathbf{W}}_{\mathbf{k}}(t^n)\}$, the spectral scheme reads

$$(3.29b) \qquad\qquad\qquad \mathbf{W}_\Delta^{n+1} = \mathbb{M}^{-1}\mathbb{A}(\mathbf{W}_\Delta^n) + \Delta t\mathbf{G}_\Delta^n.$$

The global character of spectral basis functions may yield a dense mass matrix, $\mathbb{M}$. To avoid it, one may use *preconditioning* matrices, which "approximately" invert $\mathbb{M}$; for a whole library of such preconditioning matrices we refer to, for example, [92, 216, 179].

3.5. **Which method to use?** In sections 3.1 through 3.4, we discussed the four main classes of numerical methods for PDEs: finite-difference, finite-element, finite-volume, and spectral methods. These numerical methods, together with their own toolkits, provide general, all-purpose tools for the approximate solution for general nonlinear PDEs. There is no recipe to determine which of these methods is most suitable for a given nonlinear PDE problem: most researchers will agree that there is no one superior method except, of course, the one they happen to be using in their current problem. Each method has advantages and disadvantages which were briefly mentioned above and are elaborated in the vast literature. In many applications, users may employ different ingredients of these methods to produce a numerical scheme, which is tailored to a specific problem, in order to gain overall efficiency, achieve higher-resolution, or ensure a sound theoretical basis using the concepts that are outlined in Section 4 below.

Moreover, beyond the four main classes of numerical methods discussed above, there are other methods which focus on specific families of nonlinear PDEs so that they can offer a more "faithful" description of the equations they are supposed to approximate. There is a variety of highly sophisticated, modern numerical methods, which are tied to the specific character of the underlying nonlinear PDEs. We mention our subjective choice of the top ten.

Particle methods are mesh-free methods that are used to trace the dynamics of singularities and approximate diffusive and dispersive phenomena [172, 147, 65, 39].

The *particle-in-cell* (PIC) method was advocated in computational plasma physics [63].

The class of *vortex methods* are used to simulate incompressible and slightly compressible flows [41, 65].

The *immersed boundary method*, which originated in the context of bioflows [167], traces the time evolution of the boundary of elastic structures which are immersed in incompressible fluids [168].

The *level-set method* [160, 184, 161] is used for tracking interfaces and shapes by realizing them in as the zero-level set of higher-dimensional smooth surfaces.

The *front tracking method* was developed by Glimm and collaborators [87, 105], where a separate grid is used to mark and trace the interface whereas a fixed grid is used in between these interfaces.

Wavefront methods and the *moment method* [74] are encountered in high-frequency computations, offering an alternative to traditional geometrical optics techniques based on ray tracing.

An important component in the solution of a nonlinear "problem" is the discrete geometry associated with it. There are several numerical methods which focus on this aspect of the problem, and we mention the most important two.

In *domain decomposition methods* [213] one decomposes a given boundary-value problem into a system of smaller problems supported on sub-domains which are carefully matched at their interfaces.

In *adaptive mesh refinement* (AMR) [15] one links a local refinement of the underlying grid to gain better resolution wherever the numerical solution develops large gradients.

4. Basic concepts in the analysis of numerical methods

The computed solution of a numerical scheme does *not* solve approximately the corresponding nonlinear PDE. Instead, numerical solutions are obtained as *exact* solutions of numerical schemes which are approximate models for the underlying PDEs (we ignore roundoff errors). This observation immediately leads to the following fundamental questions:

(i) In what sense does a numerical scheme approximate the underlying PDE? The answer is quantified by the notion of *consistency*.

(ii) Let $\mathbf{W}_\Delta$ be the solution of a numerical scheme, which is an approximation of the nonlinear boundary-value problem (2.1). In what sense does $\mathbf{W}_\Delta$ approximate the exact solution of the PDE, $\mathbf{w}(\cdot)$? Similarly, if $\mathbf{W}_\Delta^n$ is the numerical solution of an approximate nonlinear time-dependent scheme, then in what sense does $\mathbf{W}_\Delta^n$ approximate the corresponding exact solution $\mathbf{w}(t^n, \cdot)$? In other words, how do we know that by solving a numerical model which is "nearby" the exact differential equation, we obtain a numerical solution which is nearby the solution of the exact problem? This is the question of *convergence.*

We address these questions in the context of the numerical methods outlined above. All numerical methods are realized over finite-dimensional spaces which involve small discretization scales. Finite-difference methods are realized in terms of gridvalues, $\mathbf{W}_\Delta^n = \{\mathbf{W_j}(t^n)\}$, and relations of their divided differences over small Cartesian cells of size $\Delta = |\Delta\mathbf{x}|$. Finite-element methods are expressed in terms of piecewise polynomial basis functions, $\sum \mathbf{W}_j(t^n)\varphi_j(x)$, which are supported over local elements or cells of small size, $\Delta = \max_j \operatorname{diam} T_j$. In this case, $\mathbf{W}_\Delta^n = \{\mathbf{W}_j(t^n)\}$ are realized in terms of the pointvalues at preselected nodes of T_j. Finite-volume methods are expressed in terms of cell averages, $\mathbf{W}_\Delta^n = \{\overline{\mathbf{W}}_j(t^n)\}$ (and possibly higher-order moments) over general polyhedral cells of size $\Delta = \max_j \operatorname{diam} T_j$. Spectral methods use global polynomials of increasing degree N, which could be expressed in terms of their gridvalues, $\mathbf{W}_\Delta^n = \{\mathbf{W}(t^n, \mathbf{x_j})\}$, or their spectral content, $\mathbf{W}_\Delta^n = \{\widehat{\mathbf{W}}_{\mathbf{k}}(t^n)\}$; in this case, $\Delta = 1/N$ is the small discretization parameter. We can write this collection of different numerical methods in one of the following two abstract forms.

The implementation of different numerical methods for boundary-value problems ends up with a numerical scheme, which amounts to one of the nonlinear systems of algebraic equations, (3.10a), (3.17a), (3.24a), or (3.29a):

$$(4.1a) \qquad\qquad\qquad \mathbb{A}(\mathbf{W}_\Delta) = \mathbf{G}_\Delta.$$

Similarly, numerical methods for time-dependent problems end up with one of the evolutionary schemes, (3.10b), (3.17b), (3.24b), or (3.29b):

$$(4.1b) \qquad\qquad \mathbf{W}_\Delta^{n+1} = \mathbb{M}^{-1}\mathbb{A}(\mathbf{W}_\Delta^n) + \Delta t \mathbf{G}_\Delta^n.$$

The numerical schemes (4.1a) and (4.1b) express the relation between the computed gridvalues, cell averages, spectral coefficients, etc., and their numerical derivatives of order $|\mathbf{j}| \leq s$. In the previous sections we have seen how each numerical method uses its own "recipe" for computing numerical derivatives, based on appropriate stencils, which are characteristic to that numerical method.

4.1. **Consistency and order of accuracy.** Let $\mathbf{w}(\mathbf{x})$ be the solution of the PDE (2.1). The amount by which $\mathbf{w}(\mathbf{x})$ fails to satisfy the discrete approximation (4.1) is called the *local truncation error.* To quantify this statement, we need to *realize the exact solution over the computational grid*, Ω_Δ. Different numerical methods employ different ways to realize exact solutions. In the case of finite-difference methods, for example, the exact solution is typically realized in terms of its discrete pointvalues, $\mathbf{w}_\Delta^n = \{\mathbf{w_j}(t^n)\}$, at the Cartesian gridpoints Ω_Δ. Finite-element methods can use the discrete pointvalues of the exact solution, $\{\mathbf{w_j}(t^n)\}$, or employ the FEM projection of the exact solution, $\mathbf{w}_\Delta^n = \sum \mathbf{w}_j(t^n)\varphi_j(\mathbf{x})$. Similarly, finite-volume methods typically employ the *exact* cell averages $\mathbf{w}_\Delta^n = \{\overline{\mathbf{w}}_j(t^n)\}$ associated

with $\Omega_\Delta = \{T_j\}$ to form the FV projection $\mathbf{w}_\Delta^n(\mathbf{x}) = \sum \overline{\mathbf{w}}_j(t^n)\varphi_j(\mathbf{x})$, and spectral methods use the spectral data of the exact solution, $\mathbf{w}_\Delta^n = \{\widehat{\mathbf{w}}_\mathbf{j}(t^n)\}$ to realize the projection of the exact solution, $\mathbf{w}_\Delta^n(\mathbf{x}) = \sum \widehat{\mathbf{w}}_\mathbf{j}(t^n)p_\mathbf{j}(\mathbf{x})$.

We let $\mathbf{w}_\Delta^n$, and respectively, $\mathbf{w}_\Delta$ denote the various discrete realizations of exact solutions described above, with, or respectively, without time-dependence. Thus, $\mathbf{w}_\Delta^n$ and $\mathbf{w}_\Delta$ are viewed as projections of the exact solutions over the computational domain, Ω_Δ, and we shall use these projections of the exact solutions to quantify the local truncation errors. We distinguish between two cases. For boundary-value problems, the local truncation error of the numerical scheme (4.1a) is given by

$$(4.2a) \qquad \{\text{local error}\} := \mathbb{A}(\mathbf{w}_\Delta) - \mathbf{G}_\Delta.$$

For time-dependent problems, the local truncation error of the numerical scheme (4.1b) is given by

$$(4.2b) \qquad \{\text{local error}\} := \frac{\mathbf{w}_\Delta^{n+1} - \mathbb{M}^{-1}\mathbb{A}(\mathbf{w}_\Delta^n)}{\Delta t} - \mathbf{G}_\Delta^n.$$

In both cases, the local error depends on the small discretization parameter, Δ.

Definition 4.1 (Consistency and order of accuracy). Fix a vector norm $\|\!|\!|\cdot|\!|\!\|$. We say that the numerical scheme (4.1) is an accurate approximation of the PDE (2.1) of order $r > 0$ if, for all solutions of (2.1), the corresponding local error (4.2) is of order $\mathcal{O}(\Delta^r)$.

We distinguish between two cases.

  (i) *Boundary-value problems.* The numerical scheme (4.1a) is an approximation of order r of the boundary-value problem (2.1) if

$$(4.3a) \qquad \|\!|\!|\mathbb{A}(\mathbf{w}_\Delta) - \mathbf{G}_\Delta|\!|\!\| \lesssim \Delta^r.$$

  (ii) *Time-dependent problems.* The numerical scheme (4.1b) is an approximation of the time-dependent problem (2.1) of order $r = (r_1, r_2)$ if

$$(4.3b) \qquad \left|\!\left|\!\left| \frac{\mathbf{w}_\Delta^{n+1} - \mathbb{M}^{-1}\mathbb{A}(\mathbf{w}_\Delta^n)}{\Delta t} - \mathbf{G}_\Delta^n \right|\!\right|\!\right| \lesssim \Delta^{r_1} + (\Delta t)^{r_2}.$$

A numerical scheme is *consistent* if it is accurate of order $r > 0$.

The definition of accuracy tells us that as we *refine* the underlying grid of an accurate finite-difference method or an accurate finite-element or finite-volume triangulation, or increase the number of spectral modes, etc., the numerical scheme (4.1) becomes a more "faithful" representation of the nonlinear PDE (2.1). Of course, the higher r is, the "closer" (4.1) gets as a representation of (2.1). This, however, does not necessarily imply that the numerical solution gets "closer" to the exact solution of the PDE: consistency alone will not suffice for convergence.

It is a straightforward matter to verify the order of accuracy of a given numerical scheme. For example, the centered difference is second-order accurate:

$$(4.4a) \qquad \left|\!\left|\!\left| \frac{\mathbf{w}_{j+1,k} - \mathbf{w}_{j-1,k}}{2\Delta x} - \partial_x \mathbf{w}(x_j, y_k) \right|\!\right|\!\right| \lesssim (\Delta x)^2.$$

Larger stencils can be used to *design* difference approximations of derivatives to any order of accuracy. Similarly, the derivatives of piecewise linear polynomials used

in finite-element schemes, yield first-order accurate approximations of the exact gradients,

$$(4.4b) \qquad \left\|\nabla_{\mathbf{x}} \sum_j \mathbf{w}_j \varphi_j(\mathbf{x}) - \nabla_{\mathbf{x}} \mathbf{w}(\mathbf{x})\right\| \lesssim \Delta, \qquad \Delta = \max_j \operatorname{diam}(T_j).$$

An extensive catalog is available for finite-element discretizations with a higher-order of accuracy [43, 114, 44], or the systematic derivation of FEM stencils in [5] and the references therein. Finite-volume methods enable us to reconstruct high-order approximants from the computed cell averages. For example, the piecewise linear FV approximation we met in (3.21),

$$(4.4c) \qquad \left\| \sum_j \left(\overline{\mathbf{w}}_j + (x - x_j)(\mathbf{w}')_j \right) \mathbf{1}_{I_j}(x) - \mathbf{w}(x) \right\| \lesssim (\Delta x)^2,$$

is a second-order accurate approximation, provided the numerical derivatives are properly reconstructed so that $(\mathbf{w}')_j \approx \mathbf{w}'(x_j)$. The global stencils of spectral methods based on $N \sim 1/\Delta$ modes enjoy exponential accuracy:

$$(4.4d) \qquad \left\| D_{\mathbf{x}}^m \sum_{\mathbf{k}} \widehat{\mathbf{w}}_{\mathbf{k}}(t) e^{i\mathbf{k}\cdot\mathbf{x}} - D_{\mathbf{x}}^m \mathbf{w}(\mathbf{x}) \right\| \lesssim e^{-\sqrt[\theta]{\eta/\Delta}}, \qquad \eta > 0, \ \theta \in (0,1].$$

Remark on accuracy and smoothness. What norms should be employed to measure the accuracy in (4.3) and (4.4)? The standard notion of accuracy requires the exact solution to be *sufficiently smooth*, so that one can measure the local error in the usual pointwise sense, using the uniform L^∞-norm. Thus, for example, (4.4b) holds for twice differentiable $\mathbf{w}$'s and (4.4d) for analytic ones. On the other hand, one can interpret the notion of accuracy for less regular solutions, provided the error is measured in "weaker" norms. For example, (4.4a) and (4.4c) hold for L^2-solutions, when the error is measured in negative Sobolev (semi-)norm $W^{-2}(L^\infty)$.

4.2. **Convergence and convergence rate.** The question of convergence is of prime interest in the construction, analysis, and, of course, the implementation of numerical methods. Here, one would like to secure the convergence of the approximate solution to the exact one, as we refine the computational grid by letting $\Delta \downarrow 0$.

Definition 4.2 (Convergence and convergence rate). Fix a vector norm $\|\cdot\|$.

(i) *Boundary-value problems.* Consider the numerical scheme (4.1a) as a consistent approximation of the PDE (2.1). Let $\mathbf{W}_\Delta = \{\mathbf{W}_\Delta(\mathbf{x}) \mid \mathbf{x} \in \Omega_\Delta\}$, denote the numerical solution and let $\mathbf{w}(\mathbf{x})$ be the exact solution of (2.1), which is realized by a discrete projection, $\mathbf{w}_\Delta = \{\mathbf{w}_\Delta(\mathbf{x}) \mid \mathbf{x} \in \Omega_\Delta\}$. We say that $\mathbf{W}_\Delta$ *converges* to the exact solution, $\mathbf{w}$, if there exists $q > 0$ such that

$$(4.5a) \qquad \|\mathbf{W}_\Delta - \mathbf{w}_\Delta\| \lesssim \Delta^q, \qquad q > 0.$$

(ii) *Time-dependent problems.* Similarly, the solution of the time-dependent numerical scheme (4.1b) converges to $\mathbf{w}(t,\mathbf{x})$ if there exists $q = (q_1, q_2) > 0$ such that

$$(4.5b) \qquad \|\mathbf{W}_\Delta^n - \mathbf{w}_\Delta^n\| \lesssim \Delta^{q_1} + (\Delta t)^{q_2}, \qquad t^n \in [0,T].$$

The exponents q, q_1, q_2 quantify the convergence *rate* of the numerical scheme (4.1).

Remark on convergence and smoothness. The notion of convergence is an asymptotic statement: as we refine the grid or increase the number of modes, etc., we expect the numerical solution to get closer to the exact solution. As before, the notion of convergence requires the exact solution to be *sufficiently smooth*, depending on the norm, $\| \cdot \|$, one uses to measure the convergence rate in (4.5). We say that a numerical scheme converges if the sequence of numerical solutions converges for a sufficiently large class of exact data. Ideally, as the order of accuracy of a numerical scheme increases, we expect its convergence *rate* to improve, e.g., $q = r$. But in fact, the solution of accurate schemes need not converge at all. This brings us to the third main concept of *stability*.

4.3. Stability of numerical methods. The solution of a numerical scheme, $\mathbf{W}_\Delta^n$, is uniquely determined by the prescribed data: which consists of the boundary data and source term, $\mathbf{G}_\Delta$, the initial values, $\mathbf{W}_\Delta^0$, as well as other data supplied with the underlying PDE. The numerical scheme is *stable* if a change of the data leads to a *comparable* change in the numerical solution. To this end, we fix two vector norms, $\| \cdot \|$ and $\|\|\cdot\|\|$, to measure these changes. The choice of the possibly two different norms, $\| \cdot \|$ and $\|\|\cdot\|\|$, is intimately linked to the specific nature of the problem—the underlying PDE, its discrete approximation and its realization on the computational grid. We shall say more on these choices in section 4.5.

Definition 4.3 (**Stability**). We distinguish between two cases.

(i) *Boundary-value problems.* Let $\mathbf{W}_\Delta$ be the unique numerical solution of the finite-difference, finite-element, finite-volume, or spectral schemes (3.10a), (3.17a), (3.24a), or (3.29a):

$$(4.6a) \qquad \mathbb{A}(\mathbf{W}_\Delta) = \mathbf{G}_\Delta.$$

Each of these schemes maps discrete data $\mathbf{G}_\Delta$ to a numerical solution $\mathbf{W}_\Delta$. We consider the mapping $\mathbf{G}_\Delta \mapsto \mathbf{W}_\Delta$. The numerical scheme (4.6a) is *stable* if for all (sufficiently close) pairs of admissible data,

$$\mathbf{F}_\Delta \mapsto \mathbf{U}_\Delta \quad \text{and} \quad \mathbf{G}_\Delta \mapsto \mathbf{W}_\Delta,$$

the following estimate holds, uniformly for sufficiently Δ,

$$(4.6b) \qquad \|\mathbf{W}_\Delta - \mathbf{U}_\Delta\| \lesssim \|\|\mathbf{G}_\Delta - \mathbf{F}_\Delta\|\|.$$

(ii) *Time-dependent problems.* Let $\mathbf{W}_\Delta^n$ be the unique numerical solution of the time-dependent schemes, (3.10b), (3.17b), (3.24b), or (3.29b):

$$(4.7a) \qquad \mathbf{W}_\Delta^{n+1} = \mathbb{M}^{-1}\mathbb{A}(\mathbf{W}_\Delta^n) + \Delta t \mathbf{G}_\Delta^n.$$

Each of these schemes evolves discrete data $(\mathbf{W}_\Delta^0, \{\mathbf{G}_\Delta^n\}_{t^n \in [0,T]})$ which is mapped to a numerical solution $\{\mathbf{W}_\Delta^n\}_{t^n \in [0,T]}$. We consider the mapping $(\mathbf{W}_\Delta^0, \{\mathbf{G}_\Delta^n\}_{t^n \in [0,T]}) \mapsto \{\mathbf{W}_\Delta^n\}_{t^n \in [0,T]}$. The numerical scheme (4.7a) is *stable*, if for all (sufficiently close) pairs of admissible data,

$$\left\{\mathbf{U}_\Delta^0, \{\mathbf{F}_\Delta^n\}_{t^n \in [0,T]}\right\} \mapsto \{\mathbf{U}_\Delta^n\}_{t^n \in [0,T]} \quad \text{and} \quad \left\{\mathbf{W}_\Delta^0, \{\mathbf{G}_\Delta^n\}_{t^n \in [0,T]}\right\} \mapsto \{\mathbf{W}_\Delta^n\}_{t^n \in [0,T]},$$

the following estimate holds uniformly for sufficiently small Δ and Δt:

$$(4.7b) \qquad \|\mathbf{W}_\Delta^n - \mathbf{U}_\Delta^n\| \lesssim \|\mathbf{W}_\Delta^0 - \mathbf{U}_\Delta^0\| + \sum_{m=0}^{n} \|\|\mathbf{G}_\Delta^m - \mathbf{F}_\Delta^m\|\|, \qquad t^n \in [0,T].$$

The notion of stability is a discrete analog of the notion of well-posedness of the underlying PDE discussed in section 2.3. The stability estimates (4.6b) and (4.7b) tell us that a small perturbation of the data, measured by the norm $\|\|\cdot\|\|$, leads to a comparably small change in the corresponding numerical solutions, measured in norm $\|\cdot\|$. In particular, the stability of a numerical scheme (4.6b) enables us to compare its numerical solution, $\mathbf{W}_\Delta$, with the discrete projection of the *exact* solution, $\mathbf{w}_\Delta$. Indeed, by consistency, (4.2a), the discrete projection of the exact solution, $\mathbf{w}_\Delta$, satisfies the same numerical scheme as $\mathbf{W}_\Delta$ does, modulo the perturbed data due to local truncation errors,

$$\mathbf{G}_\Delta + \{\text{local error}\} \; \mapsto \mathbf{w}_\Delta.$$

Similarly, in the case of a consistent time-dependent scheme (4.2b), the discrete projection of the exact solution, $\mathbf{W}_\Delta^n$, solves the perturbed numerical scheme

$$\mathbf{G}_\Delta^n + \Delta t \cdot \{\text{local error}\} \; \mapsto \mathbf{w}_\Delta^n.$$

Stability implies that the difference between the computed solution and the discrete projection of the exact solution, $\mathbf{W}_\Delta - \mathbf{w}_\Delta$ and $\mathbf{W}_\Delta^n - \mathbf{w}_\Delta^n$, is dictated by the size of the *local errors*: by the assumption of consistency, they rapidly tend to zero. We can summarize this argument as follows.

Theorem 1 (Stability implies convergence of consistent schemes). *Let $\mathbf{W}_\Delta$ be the solution of a numerical method* (4.6a), *consistent with a well-posed boundary-value problem* (2.1); *in particular, assume that it is accurate of order $r > 0$, i.e.,* (4.3a) *holds. Then, if the numerical method* (4.6a) *is stable* (4.6b), *its solution converges with rth-order convergence rate,*

$$(4.8a) \qquad\qquad\qquad \|\mathbf{W}_\Delta - \mathbf{w}_\Delta\| \lesssim \Delta^r.$$

Similarly, let $\mathbf{W}_\Delta^n$ be the solution of a numerical method (4.7a) *consistent with a well-posed time-dependent problem* (2.1); *in particular, assume that it is accurate of order $r > 0$, i.e.,* (4.3b) *holds. Then, if the numerical method* (4.7a) *is stable* (4.7b), *its solution converges with rth-order convergence rate,*

$$(4.8b) \quad \|\mathbf{W}_\Delta^n - \mathbf{w}_\Delta^n\| \lesssim \sum_{m=0}^{n} \Delta t \cdot \|\|\{\text{local error}\}\|\| \lesssim \Delta^{r_1} + (\Delta t)^{r_2}, \qquad t^n \in [0, T].$$

Remark on discrete projections. Observe that (4.8) does not involve the exact solution of the PDE, $\mathbf{w}(\mathbf{x})$ and $\mathbf{w}(t^n, \mathbf{x})$. Instead, it establishes convergence toward their discrete projections, $\mathbf{w}_\Delta$ and $\mathbf{w}_\Delta^n$. The remaining differences, $\mathbf{w}(\cdot) - \mathbf{w}_\Delta(\cdot)$, and similarly, $\mathbf{w}(t^n, \cdot) - \mathbf{w}_\Delta^n(\cdot)$, depend on the type of numerical realization, and their convergence is dictated solely by

   (i) the regularity of the underlying solutions; and
   (ii) the specific norm, $\|\cdot\|$ used to measure the difference between an exact solution and its discrete projection.

It seems that this type of error, $\|\mathbf{w}(\cdot) - \mathbf{w}_\Delta(\cdot)\|$, which *must be* made by the mere representation of an infinite-dimensional exact solution over the finite-dimensional computational grid, will dominate the overall convergence rate, $\|\mathbf{w}(\cdot) - \mathbf{W}_\Delta(\cdot)\|$. This, however, need not be the case. Once again, the choice of the norm $\|\cdot\|$ plays an essential role here. We clarify this point with an example of spectral approximations. Consider the Fourier projection, $\mathbf{w}_\Delta(\mathbf{x}) = \sum_{|\mathbf{k}| \leq N} \widehat{\mathbf{w}}_\mathbf{k} e^{i\mathbf{k}\cdot\mathbf{x}}$, of a certain

exact solution, $\mathbf{w}(\mathbf{x})$. If $\mathbf{w}(\mathbf{x})$ contains discontinuities, then the *representation error*, $\|\mathbf{w}_\Delta(\cdot) - \mathbf{w}(\cdot)\|_{L^p}$ is at most first-order accurate due to the Gibbs phenomena [199]. However, when measured in negative Sobolev (semi-)norm, one recovers the high accuracy of the Fourier projection, $\|\mathbf{w}_\Delta(\cdot) - \mathbf{w}(\cdot)\|_{H^{-s}} \lesssim N^{-s-1}$. Thus, the representation error does not necessarily dominate the convergence rate, when measured by proper "weak" norms. The information content in highly accurate approximations of "rough" data can be extracted by postprocessing [129, 151, 199]. Figure 3.11(b) demonstrates how such postprocessing extracts the information from the oscillatory SV solution in Figure 3.11(a).

Stability plays a central role in the theory of numerical methods. It shifts the burden of a convergence proof into the concept of stability, which in turn depends solely on the properties of the numerical scheme, but otherwise does *not* involve the underlying PDE. The compatibility between the two—the numerical scheme and the underlying PDE it approximates—is guaranteed by the easily checkable notion of consistency. However, a convergence argument along these lines faces two main *practical* difficulties. In generic cases, the norms employed by the stability estimates (4.6b), (4.7b) are dictated by similar well-posedness estimates of the underlying PDEs, and the local errors need *not* be small when measured in these norms. A second, more notorious difficulty, is that the well-posedness of PDEs in the sense of their continuous dependence on the data is often not known. Consequently, the stability estimates sought in (4.6b) and (4.7b) are too difficult to establish. This is particularly relevant in the nonlinear setup. One therefore seeks weaker stability assumptions. A prototype example is the assumption of *boundedness*.

Definition 4.4 (Stability revisited—boundedness). Fix two vector norms, $\|\cdot\|$ and $\|\|\cdot\|\|$.

(i) *Boundary-value problems.* Let $\mathbf{W}_\Delta$ be the numerical solution of the boundary-value, finite-difference, finite-element, finite-volume, or spectral scheme (3.10a), (3.17a), (3.24a) or (3.29a):

(4.9a) $$\mathbb{A}(\mathbf{W}_\Delta) = \mathbf{G}_\Delta.$$

The numerical scheme (4.9a) is *bounded* if the following estimate holds uniformly for sufficiently Δ:

(4.9b) $$\|\mathbf{W}_\Delta\| \lesssim \|\|\mathbf{G}_\Delta\|\|.$$

(ii) *Time-dependent problems.* Let $\mathbf{W}_\Delta^n$ be the numerical solution of the homogeneous time-dependent scheme, (3.10b), (3.17b), (3.24b) or (3.29b) with $\mathbf{G}_\Delta^n$:

(4.10a) $$\mathbf{W}_\Delta^{n+1} = \mathbb{M}^{-1}\mathbb{A}(\mathbf{W}_\Delta^n).$$

The numerical scheme (4.10a) is *bounded* if the following estimate holds uniformly for sufficiently small Δ and Δt:

(4.10b) $$\|\mathbf{W}_\Delta^n\| \lesssim \|\mathbf{W}_\Delta^0\|, \qquad t^n \in [0, T].$$

Remark on the notion of boundedness. There is more than just one notion of boundedness with respect to the data. In boundary-value problems, one can measure boundedness with respect to the boundary data $\mathbf{b}_\Delta$, the inhomogenous data $\mathbf{G}_\Delta$, or with respect to both as sought in (4.9b). Similarly, boundedness in time-dependent problems can be measured with respect to the initial data as sought

in (4.10b), with respect to the boundary and inhomogeneous data (a resolvent type estimate, e.g., [95]), or with respect to both.

The bounds in (4.9b) and (4.10b) tell us that if the data are inside a small ball around the origin, then the corresponding numerical solution cannot be arbitrarily large: it should be inside a ball of a comparable size. This is clearly *necessary* to guarantee convergence. Otherwise, the numerical solution may grow arbitrarily large, despite the vanishing size of the data which are associated with the (typical) zero solution $\mathbf{w} \equiv 0$. Thus, we view the bounds (4.9), (4.10) as a measure of stability with respect to the special zero data (and in a more general setup, one may employ other special "preferred" data). In certain cases, boundedness is also sufficient to guarantee the convergence. We mention two important cases.

(i) The implication "boundedness $\implies$ convergence" can be argued in certain nonlinear cases, where the bounds (4.9b) and (4.10b) hold with a norm, $\|\cdot\|$, which is "strong enough" to guarantee the *compactness* of the family of numerical solutions, $\{\mathbf{W}_\Delta\}$ or $\{\mathbf{W}_\Delta^n\}$, and the (numerical) derivatives involved in the numerical scheme. It follows that there is a converging subsequence as $\Delta \downarrow 0$, and consistency then implies that this limit must be the desired solution of the underlying PDE. This line of argument yields convergence, $\|\mathbf{W}_\Delta^n(\mathbf{x}) - \mathbf{w}(t^n, \mathbf{x})\| \xrightarrow{\Delta \to 0} 0$, but it lacks convergence rate estimates. As examples, we mention the convergence proofs of the Glimm finite-difference approximation [86] based on a total-variation bound, the convergence of finite-difference and finite-element approximations of the incompressible Euler and Navier–Stokes equation based on an energy bound [40, 114, 51], or the convergence of finite-volume and spectral schemes based on their entropy production bounds [53, 48, 77, 195].

(ii) The implication "boundedness $\implies$ convergence" applies to the general case of *linear* schemes. The numerical schemes (4.9a), (4.10a) are *linear* if the matrices $\mathbb{M}$ and $\mathbb{A}$ are. In the linear case, the notion of boundedness is *equivalent* with the notion of stability,[2] which brings our discussion to the linear setup.

4.4. From the linear to the nonlinear setup.
We have a fairly solid understanding of the *linear theory* for numerical methods for PDEs. Several key concepts from the linear setup apply to nonlinear PDEs, as long as the underlying solutions involved are sufficiently smooth. We mention a few of them.

FEMs for *linear boundary-value problems* are typically formulated within the "weak" framework of the Lax–Milgram lemma, and are realized by Galerkin or Ritz methods. There is an extensive "catalog" of conformal and nonconformal elements which are chosen to be compatible with constraints of the underlying PDEs. Convergence is quantified in terms of the Céa and Bramble–Hilbert lemmas [43, 114, 25]. Stability of mixed-type FEMs for saddle-point problems is verified in terms of the Babuška–Brezzi *inf-sup condition* [8, 26]. The finite elements are adapted to local variations of the solution: adaptivity is often tuned by a posteriori estimates [14, 22, 157].

Finite-difference methods for *linear time-dependent problems* come in several flavors of dissipative or unitary schemes, explicit or implicit schemes [122, 123]. Notable examples are the dissipative Lax–Friedrichs and Lax–Wendroff schemes, the unitary Leap-Frog scheme and the implicit backward Euler and Crank–Nicolson

---

[2]Often, therefore, one finds in the literature the distinction between the *nonlinear stability* estimates (4.6), (4.7), and the *linear stability* bounds, (4.9), (4.10).

schemes [175, 95]. The computation of multidimensional probelms is often accomplished using splitting methods such as Strang splitting and alternating direction implicit methods [175, 181]. Linear stability in the sense that the bound (4.10b) holds, can be checked by von Neumann stability analysis. The notion of linear stability is strong enough to guarantee stability against perturbations of the inhomogenous data (4.7b),

$$(4.10b) \quad \mapsto \quad \|\mathbf{W}_\Delta^n - \mathbf{U}_\Delta^n\| \lesssim \|\mathbf{W}_\Delta^0 - \mathbf{U}_\Delta^0\| + \sum_{m=0}^{n} \|\mathbf{G}_\Delta^m - \mathbf{F}_\Delta^m\|, \qquad t^n \in [0, T],$$

which in turn yields (one half of) the celebrated Lax–Richtmyer equivalence theorem [133].

Theorem 2 (**Stability and convergence are equivalent for linear problems**). *Let $\mathbf{W}_\Delta^n$ be the solution of a linear numerical scheme* (4.10a) *consistent with a well-posed linear time-dependent problem* (2.1). *Then, stability* (4.10b) *is necessary and sufficient for convergence.*

The implication "stability $\implies$ convergence" played a central role in the early years of development of numerical methods for PDEs [175, Sec. 3.5]. As we already mentioned, it shifts the burden of proving convergence into a proof of stability, which in turn depends solely on the properties of the numerical method, but otherwise does *not* involve the underlying PDE. A more quantitative approach [95, Sec. 5.1] implies that the *convergence rate*, $\|\mathbf{W}_\Delta^n - \mathbf{w}_\Delta^n\|$, is of the same order expected by the order of consistency, namely, $q = r$. In the linear case, the assumption of stability is more accessible than nonlinear stability: the bound (4.9b) amounts to the *uniform* invertibilty of $\mathbb{A}$; the bound (4.10b) amounts to the *uniform* power-boundedness, $(\mathbb{M}^{-1}\mathbb{A})^n$, or the *uniform* product-boundedness, $\Pi_n \mathbb{M}^{-1}\mathbb{A}(t^n)$. The bounds should hold *uniformly* with respect to $\Delta \downarrow 0$. The inverse implication of the equivalence theorem, "convergence $\implies$ stability," follows from general principles for families of bounded linear operators.

The celebrated theorem of Strang [189] guarantees that linear stability carries over to the *nonlinear setup*, as long as the underlying solution involved is sufficiently smooth.

4.5. Challenges in numerical methods for nonlinear problems. Unlike the linear setup, one cannot expect to have a unified framework to analyze the convergence of numerical methods for nonlinear PDEs. If the solution of the nonlinear PDE we are interested in approximating is sufficiently smooth, then the linear convergence theory usually prevails. Thus, the main challenge is solving nonlinear problems which come with a *limited degree of smoothness*. The challenges vary between different nonlinearities, depending on special feature of the problem at hand. We mention two aspects of such challenges.

(i) **Local and global invariants**. Often, the solutions of problems with a limited degree of smoothness have a restricted phase space, with values that lie in a region or a lower-dimensional manifold, $\Sigma \subset \mathbb{R}^p$, such that $\mathbf{w}(\mathbf{x}) \in \Sigma$ for all $\mathbf{x} \in \Omega$. In particular, nonlinear time-dependent problems are often endowed with *invariant regions*, $\Sigma \subset \mathbb{R}^p$, such that the nonlinear solution operator satisfies $\mathbf{w}_0(\cdot) \in \Sigma \mapsto \mathbf{w}(t, \cdot) \in \Sigma$. To compensate for the loss of smoothness, it is essential to design numerical approximations which respect the corresponding local invariants, namely, their numerical solutions should stay in or nearby the preferred region,

$\mathbf{W}_\Delta \in \Sigma_\Delta$. As examples we mention properties of positivity, maximum principle, convexity, etc. Other local invariants could come as differential forms carried out by the exact solution, $M(\partial, \mathbf{w}, \mathbf{x}) \in \Sigma \subset \mathbb{R}^p$. As examples we mention constraint-transport, which preserves incompressibility and other trace-free flows, irrotational flows, topological degree, variational inequalities, and entropy inequalities.

Another important class of invariants which is essential in many nonlinear numerical methods is the class of *global invariants*. As examples we mention the conservation of mass, which is the basic framework for modern "shock-capturing" methods, the class of *conservative schemes* in the sense of Lax–Wendroff [134]; *Energy conservative* schemes which are advocated in long-term calculations of weather prediction using the global circulation model [3]; *entropy stable* schemes are sought as a "faithful" computations of physically relevant shock-discontinuities [198, 201], and numerical methods which preserve the *integrals of motions* for (completely) integrable systems [217, 107, 108, 7].

(ii) **On the choice of norms**. As we mentioned earlier, the stronger notion of (nonlinear) stability (4.6b), (4.7b) is difficult to verify in many nonlinear problems. This is particularly relevant for nonlinear problems with a limited degree of smoothness. At the same time, nonlinearity makes the passage from boundedness to convergence a more delicate task. The bounds (4.9b), (4.10b) on the numerical solutions $\|\mathbf{W}_\Delta\|$ and, respectively, $\|\mathbf{W}_\Delta^n\|$, do not guarantee convergence, unless the norm $\|\cdot\|$ is strong enough to enforce compactness. There are several tools to obtain such desired bounds. We mention strong compactness bounds expressed in terms of Sobolev, Hölder, or Harnack-type estimates, monotonicity bounds [75], and a host of weak compactness bounds, which involve convexity and quasi-convexity arguments, compensated compactness, Γ- and H-convergence, concentration compactness, or use of the averaging lemma [205, 138, 75, 91, 206, 84, 68, 60, 202]. The difficulty lies with the fact that these bounds often require matching the nonlinear PDE with a sufficiently weak norm $\|\cdot\|$ to measure consistency in the sense that (4.3) holds. Thus, the passage from linear or nonlinear stability to convergence depends on what kind of norms are employed in the stability and boundedness estimates, (4.6b), (4.7b) and (4.9b), (4.10b).

So far we have not specified the norms, $\|\cdot\|$ and $\|\|\cdot\|\|$, which are to be used in the various estimates of consistency, convergence, and stability. For example, the size of the local error in (4.2) should be measured by an appropriate norm, $\|\|\cdot\|\|$, which is compatible with the underlying PDE, the underlying grid, and the specific numerical method being employed. The upper bounds on the local error on the right of (4.3) then depend on the smoothness of $\mathbf{w}$, which in turn requires a higher-order Sobolev norm involving $\|\|\partial^{\boldsymbol{\beta}} \mathbf{w}\|\|$. Similarly, convergence in (4.5) and stability estimates (4.6b), (4.7b) should be measured with respect to appropriate norms, which are compatible with the underlying nonlinear PDE. A few examples are in order.

In the linear case, the stability of numerical schemes for problems of hyperbolic type is typically analyzed in terms the L^2-norm [133, 122, 132, 189]. Problems of parabolic and elliptic type use the uniform, L^∞-norm [209]. The stability of systems which arise from a mixed formulation of an FEM is often achieved in terms of Babuška–Brezzi *inf-sup condition* [8, 26], where stability is measured in terms of the H^1- and H^{-1}-norms, or similar pairs of dual norms, $\|\cdot\|$ and $\|\|\cdot\|\|$. The well-posedness of nonlinear conservation laws and related equations is typically achieved

in the L^1-norm, and numerical stability is therefore sought in the L^1-metric [21]. In this case, one has L^1-stability against perturbations which in turn implies the bounded variation (BV)-stability [90, 100]. The theory of viscosity solutions for nonlinear Hamilton–Jacobi and fully nonlinear elliptic equations was developed in the L^∞-framework [57, 30], as are the corresponding convergence theories [188, 158, 31]. To overcome the lack of smoothness, one can use negative Sobolev norms $\|\|\cdot\|\|_{W^{-m}(L^p)}$ [151, 196, 85]. In certain cases, one must measure the errors which are supported only on the computational grid, using *discrete norms* such as ℓ^2. In other cases, one may need to carefully adjust the measure of local errors using norms which are compatible with *adaptive* grids [22]. Nonlinear Schrödinger equations and related semilinear dispersive equations were studied using mixed space-time Strichartz $L_t^q L_x^p$ norms [204], and the stability of numerical methods follows along the same lines.

We conclude by noting that although the definition of stability does *not* involve the underlying PDEs, the framework enforced by a choice of a proper norm makes a fine interplay between the notion of stability of a numerical scheme and the well-posedness of the underlying PDE it tries to approximate. This interplay remains a key issue in the construction, analysis, and implementation of numerical methods for nonlinear PDEs.

5. Future directions

There are three main sources of influence on new developments in numerical methods for nonlinear PDEs.

Mathematical models and modern mathematical tools. A large portion of the theory of PDEs was developed in response to models that originated in the physical sciences. Just as the Laplace equation, the wave equation, and the heat equation are prototypical linear PDEs, the minimal surface equation, the Schrödinger equation, and Navier–Stokes equations are canonical examples that are driving much of the study of nonlinear PDEs. A parallel development of numerical methods follows. In recent decades, a growing part of the theory was expanded to include nonlinear PDEs driven by models from social and biological sciences. These models lack the precise foundations of Newton's, Maxwell's, or Schrödinger's equations. Instead, there is a growing role for nonlinear *stochastic* PDEs [112, 146, 42] with a wide range of applications, from financial models and data assimilation in atmospheric sciences to material sciences and biological models; see [118, 185, 116, 121, 154, 169, 166] and the references therein. Moreover, more often than not, realistic models from social and biological sciences do *not* allow separation of scales; instead, one is forced to study nonlinear PDEs *across* scales. Numerical methods for such nonlinear PDEs will therefore have to integrate stochastic aspects and will be inherently multiscale.

We should also mention the influence of modern mathematical tools on the development of new directions for numerical methods for solving such equations. As an example, we mention developments of new geometric tools in nonlinear PDEs [98, 37, 210, 164], fully nonlinear elliptic equations, optimal transportation and Navier–Stokes equations [57, 29, 218, 139] as examples which should pave the way for future developments in numerical methods.

Numerical analysis. The solution of numerical approximation of nonlinear PDEs is realized over finite-dimensional spaces—gridvalues, local moments, cell averages, etc. As such, the construction of novel numerical algorithms had a profound impact on modern developments of numerical methods for (nonlinear) PDEs. Indeed, it was well known that during the period of serial processors, the speed-up in computation due to improved hardware—the exponential graph predicted by "Moore's law" [152]—was matched by a similar graph of speed-up due to the development of novel computational algorithms. A few examples are in order: the QR algorithm for computing eigensystems [80] and the fast Fourier transform FFT [52], which gave the impetus for the development of spectral methods during the 1960s; the development of multigrid and MATLAB in the 1970s [24, 148, 36]; wavelets, linear programming interior point methods, and the fast multipole method (FMM) [61, 149, 117, 94] in the 1980s; high-resolution methods for discontinuous solutions in the 1990s [100, 49]; and curvelets, greedy algorithms, compressive sensing and other "optimal algorithms" of finite-dimensional approximations, which have matured during recent years [32, 69, 33, 208, 66].

Future developments of numerical methods for nonlinear PDEs will continue to be influenced by unknown numerical algorithms, which are yet to be developed: new tools to cope with the "curse of dimensionality", further systematic developments of adaptivity in the presence of different scales, probabilistic algorithms, and an increasing role for combinatorial aspects of the underlying algorithms are a few examples expected from future developments of numerical methods for solving nonlinear PDEs.

New computational platforms. Computers *used* to get smaller and faster, but in recent decades the direction changed towards faster computing using parallel processing, cyber computing, and using dedicated rather than all-purpose processors. Different platforms will require dedicated algorithms, which will take full advantage of new computing architectures. As a recent example, we mention the success of using graphical processing units (GPUs) in running large scale simulations much faster than multicore systems [111]. At the same time, the resulting increase in computing power will enable us to simulate more than just nonlinear PDEs at a given scale; it will enable us to model *hierarchies* of scales. We mention in this context the examples of numerical homogenization and upscaling methods [16, 109, 72], the heterogeneous multiscale method of E and Engquist [71], and the equation-free approach of Keverkidis and his coworkers [120]. The main aspect in these approaches goes beyond the numerical solution of a given model: petaflop computational platforms will enable actual modeling across the hierarchy of discrete scales. These developments will enable, in the context of numerical weather prediction, for example, a multiscale simulation of the interplay between the global circulation numerical model and highly localized dynamics. We will then get closer to realizing the full potential behind von Neumann's vision [156], where "the entire computing machine is merely one component of a greater whole, namely, of the unity formed by the computing machine, the mathematical problems that go with it, and the type of planning which is called by both."

Acknowledgments

About the author

Eitan Tadmor is a Distinguished University Professor in the department of mathematics and the director of the University Center for Scientific Computation and Mathematical Modeling at the University of Maryland, College Park. He received his education at Tel-Aviv University and CalTech, and he was a founding co-director of the NSF Institute for Pure and Applied Mathematics (IPAM) at UCLA.

References

[1] Adams, R. and Fournier, J. (2003), Sobolev spaces, 2nd ed., Academic Press. MR2424078 (2009e:46025)

[2] Alvarez, L., Lions, P. L. and Morel J. M. (1992), Image selective smoothing and edge detection by non-linear diffusion II, SIAM J. Num. Anal., Vol. 29 (3), pp. 845-866. MR1163360 (93a:35072)

[3] Arakawa, A. (1966), Computational design for long-term integration of the equations of fluid motion: two-dimensional incompressible flows. I. J.Comput. Phys. v. 1, pp. 119-143 (reprinted in v. 135, pp. 103-114) MR1486265

[4] Arnold, D. N. (1990), Mixed finite element methods for elliptic problems, Comput. Methods Appl. Mech. Engrg., 82(1-3), pp. 281-300. MR1077658 (91h:65168)

[5] Arnold, D. N., Falk, R. S. and Winther, R. (2006), Finite element exterior calculus, homological techniques, and applications, Acta Numer. 15, pp. 1-155. MR2269741 (2007j:58002)

[6] Arnold, D. N., Brezzi, F., Cockburn B., and Marini, L. D. (2002), Unified analysis of discontinuous Galerkin methods for elliptic problems, SIAM J. Numer. Anal. 39(5), pp. 1749-1779. MR1885715 (2002k:65183)

[7] Artstein, Z., Gear, C. W., Kevrekidis, I. G., Slemrod M., and Titi, E. S. (2011), Analysis and computation of a discrete KdV-Burgers type equation with fast dispersion and slow diffusion, SIAM J. Numer. Anal., v. 49(5), pp. 2124-2143. MR2861712

[8] Babuška, I. (1971), Error Bounds for Finite Element Method, Numerische Mathematik, v. 16, pp. 322-333. MR0288971 (44:6166)

[9] Babuška, I. (1973), The finite element method with Lagrangian multipliers, Numer. Math. v20, pp. 179-192. MR0359352 (50:11806)

[10] Babuška, I. and Suri, M. (1994), The p and hp versions of the finite element method, basis principles and properties, SIAM Review, v. 36, pp. 578-632. MR1306924 (96d:65184)

[11] Balbas, J. and Tadmor, E. (2010), CentPack: A package of high-resolution central schemes for non-linear conservation laws and related problems, http://www.cscamm.umd.edu/centpack/.

[12] Bao, W., Du, Q. and Zhang, Y. (2006), Dynamics of rotating Bose–Einstein condensates and its efficient and accurate numerical computation, SIAM J. Appl. Math. 66 758-786. MR2216159 (2006k:35267)

[13] Bao, W., Li, H.-L, and Shen, J. (2009), A generalized-Laguerre-Fourier-Hermite pseudospectral method for computing the dynamics of rotating Bose-Einstein condensates, SIAM J. Sci. Comput. 31, pp. 3685-3711. MR2556558 (2010j:65193)

[14] Becker, R. and Rolf Rannacher, R. (2001), An optimal control approach to a posteriori error estimation in finite element methods, Acta Numerica v. 10, pp 1-102. MR2009692 (2004g:65147)

[15] Berger, M. and Oliger, J. (1984), Adaptive mesh refinement for hyperbolic partial differential equations, J. Comput. Phys., v. 53, pp. 484-512. MR739112 (85h:65211)

[16] Bensoussan, A., Lions, J.-L. and Papanicolaou, G. (1978), Asymptotic analysis for periodic structures, Studies in Mathematics and its applications, Vol. 5, North-Holland Publishing Company. MR503330 (82h:35001)

[17] Brebbia, C. A., (1978), The Boundary Element Method for Engineers, Pentech Press/Halstead. MR806953 (87b:65192)

[18] Brebbia, C. A. and Dominguez, J. (1977), Boundary element methods for potential problems, J. Appl. Math. Model. v. 1, pp 372-378. MR0520348 (58:25017)

[19] Bernardi, C. and Maday, M. (1992), Approximations spectrales de problemes aux limites elliptiques Springer-Verlag, Paris. MR1208043 (94f:65112)

[20] Bernardi, C. and Maday, M. (1996), Spectral Element Methods, (P. G. Ciarlet and J. L. Lions, eds), Handbook of Numerical Analysis, North-Holland, Amsterdam.

[21] Bianchini, S. and Bressan, A. (2005), Vanishing viscosity solutions of non-linear hyperbolic systems. Ann. of Math. (2) 161, no. 1, pp. 223-342. MR2150387 (2007i:35160)

[22] Binev, P., Dahmen, W. and DeVore R. (2004), Adaptive finite element methods with convergence rates, Numer. Math., Vol 97(2), pp. 219-268. MR2050077 (2005d:65222)

[23] Bochev, P. and Gunzburger, M. (2006), Least-squares finite element methods, ICM 2006. Invited Lectures. Abstracts. Section 16 (Sanz-Solé M., Soria J., Varona J. L. & Verdera J. eds.), vol. III. pp. 1137-1162, EMS. MR2275722 (2008d:65131)

[24] Brandt, A. (1977), Multi-level adaptive solutions to boundary-value problems, Math. Comp, 31, pp. 333-390. MR0431719 (55:4714)

[25] Brenner, S. and Scott, R. L. (2005), The Mathematical Theory of Finite Element Methods, 2nd edition, Springer.

[26] Brezzi, F. (1974), On the existence, uniqueness and approximation of saddle-point problems arising from Lagrangian multipliers. Rev. Française Automat. Informat. Recherche Opérationnelle Sér. Rouge v. 8(2), pp. 129-151. MR0365287 (51:1540)

[27] Brezzi, F. and Fortin, M. (1991), Mixed and Hybrid Finite Element Methods, Springer Verlag. MR1115205 (92d:65187)

[28] Butcher, J. C. (2003), Numerical Methods for Ordinary Differential Equations, Wiley, 2003. MR1993957 (2004e:65069)

[29] Caffarelli, L. (2002), Non-linear elliptic theory and the Monge–Ampere equation, "International Congress of Mathematicians", Proceedings of the ICM02 Beijing 2002 (Li Tatsien, ed.), Vol. I: Plenary lectures, Higher Education Press (2002) 179-187. MR1989184 (2004d:35068)

[30] Caffarelli, L. and Cabré, X. (1995), Fully Non-linear Elliptic Equations, Colloq. Publ. Vol. 43, Amer. Math. Soc. MR1351007 (96h:35046)

[31] Caffarelli, L. and Souganidis, P. (2007), A rate of convergence for monotone finite difference approximations to fully non-linear, uniformly elliptic PDEs, Comm. Pure Appl. Math., v. 61(1), pp. 1-17. MR2361302 (2008m:65288)

[32] Candés, E. J. and Donoho, D. L. (2001), Curvelets and curvilinear integrals. J. Approx. Theory 113(1), pp. 59-90. MR1866248 (2002j:41012)

[33] Candés, E. J., Romberg, J. and Tao, T. (2006), Robust uncertainty principles: exact signal reconstruction from highly incomplete frequency information, IEEE Trans. Inform. Theory 52(2), pp. 489-509. MR2236170 (2007e:94020)

[34] do Carmo., M. P. (1976), Differential Geometry of Curves and Surfaces, Prentice Hall. MR0394451 (52:15253)

[35] Cercignani, C. (1998), The Boltzmann Equation and Its Applications, Springer Verlag. MR1313028 (95i:82082)

[36] Chan T. F., Xu, J. and Zikatanov, L. (1998), An agglomeration multigrid method for unstructured grids, Contemp. Math. v. 218, pp. 67-81. MR1645844 (99h:65205)

[37] Chang, S.-Y. A. and Yang, P. C. (2002), Non-linear partial differential equations in conformal geometry, Proc. Inter. Congress Math. Vol. I (Beijing, 2002), pp. 189-207, Higher Ed. Press, Beijing. MR1989185 (2004d:53031)

[38] Charney, J. G., Fjörtoft R. and von Neumann, J. (1950), Numerical Integration of the Barotropic Vorticity Equation, Tellus, Vol. 2, pp. 237-254. MR0042799 (13:164f)

[39] Chertock, A. and Levy, D. (2002), Particle methods for the KdV equation, J. Sci. Comput. Vol. 17, pp. 491-499. MR1910746

[40] Chorin, A. J. (1968), Numerical Solution of the Navier-Stokes Equations, Math. Comp., 22, pp. 745. MR0242392 (39:3723)

[41] Chorin, A. J (1973), Numerical study of slightly viscous flow, Journal of Fluid Mechanics, v. 57, pp. 785-796. MR0395483 (52:16280)

[42] Chorin, A. and Hald, O. (2006), Stochastic Tools in Mathematics and Sciences, Surveys Tutorials Appl. Math. Sci, vol. 1, Springer. MR2189824 (2006j:60001)

[43] Ciarlet, P. G. (1978), The Finite Element Method for Elliptic Problems, North-Holland. MR0520174 (58:25001)

[44] Ciarlet, P. G. and Lions, J. L., eds. (1991), Handbook of Numerical Analysis, Vol. II: Finite Element Methods (1991) and Vol. IV: Finite Element Methods, Numerical Methods for Solids, (1996), North-Holland, Amsterdam. MR1115235 (92f:65001)

[45] Ciarlet, P. G. and Lions, J. L., eds. (2000), Handbook of Numerical Analysis, Vol. VII: Finite Volume Methods, North-Holland, Amsterdam. MR1804744 (2001h:65001)

[46] Clay Mathematics Institute, (2000), Millennium Problems, http://www.claymath.org/millennium/.

[47] Cockburn, B. (1998), An introduction to the discontinuous Galerkin method for convection-dominated problems, Advanced numerical approximation of nonlinear hyperbolic equations (Cetraro, 1997), Lecture Notes in Math., Springer, Berlin., Vol. 1697, pp. 151-268. MR1728854 (2001f:65117)

[48] Cockburn, B., Coquel, F. and LeFloch, P. G. (1995), Convergence of finite volume methods for multidimensional conservation laws, SIAM J. Numer. Anal. 32, pp. 687-705. MR1335651 (97f:65051)

[49] Cockburn, B., Johnson, C., Shu, C.-W. and Tadmor, E. (1998), Approximate solutions of nonlinear conservation laws, in "Advanced Numerical Approximation of Nonlinear Hyperbolic Equations" C.I.M.E. course in Cetraro, Italy, June 1997 (A. Quarteroni ed.), Lecture notes in Mathematics v. 1697, Springer Verlag. MR1729305 (2000h:65004)

[50] Colella, P. and Woodward, P. (1984), The piecewise parabolic method (PPM) for gas-dynamical simulations, J. Comput. Physics 54, 174-201.

[51] Constantin, P. and Foias, C. (1988), Navier-Stokes Equations, The Univ. of Chicago Press. MR972259 (90b:35190)

[52] Cooley, J. W. and Tukey, J. W. (1965), An algorithm for the machine calculation of complex Fourier series, Math. Comput. v. 19, pp. 297-301. MR0178586 (31:2843)

[53] Coquel, F. and LeFloch, P. G. (1993), Convergence of finite difference schemes for scalar conservation laws in several space variables. General theory, SIAM J. Numer. Anal. 30 pp. 675-700. MR1220646 (94e:65092)

[54] Courant, R. (1943), Variational methods for the solution of problems of equilibrium and vibrations, Bull. AMS 49 pp. 1-23. MR0007838 (4:200e)

[55] Courant, R., Friedrichs, K. and Lewy, H. (1967), On the partial difference equations of mathematical physics, IBM Journal, vol. 11(2) pp. 215-234, English translation of the 1928 German original "Über die partiellen Differenzengleichungen der mathematischen Physik", Mathematische Annalen, Vol. 100, No. 1, pp. 32-74, 1928. MR1512478

[56] Courant, R. and Friedrichs, K.-O. (1948), Supersonic Flow and Shock Waves, Springer, New York. MR0029615 (10:637c)

[57] Crandall, M. G. and Lions, P.-L. (1983), Viscosity Solutions of Hamilton–Jacobi Equations, Transactions of the Amer. Math. Soc., v. 277(1), pp. 1-42. MR690039 (85g:35029)

[58] Crouzeix, M. and Raviart, P. A. (1973), Conforming and non-conforming finite element methods for solving the stationary Stokes equations, R.A.I.R.O. Anal. Numer. v. 7 pp. 33-76. MR0343661 (49:8401)

[59] Dafermos, C. (2010), Hyperbolic Conservation Laws in Continuum Physics, v. 325, 3rd edition, Springer. MR2574377 (2011i:35150)

[60] Dal Maso, G. (1993), An Introduction to G-convergence. Birkhäuser, Basel.

[61] Daubechies, I. (1992), Ten Lectures on Wavelets, Society for Industrial and Applied Mathematics. MR1162107 (93e:42045)

[62] Dautray, R. and Lions, J.-L. (2000), Mathematical Analysis and Numerical Methods for Science and Technology, vol. 4., Springer. MR1081946 (91h:00004b)

[63] Dawson, J. M. (1983), Particle simulation of plasmas, Reviews of Modern Physics v. 55, pp. 403.

[64] Dean, E. J. and Glowinski, R. (2004), Numerical solution of the two-dimensional elliptic Monge–Ampére equation with Dirichlet boundary conditions: a least-squares approach, Comptes Rendus Mathematique Vol. 339(12), pp. 887-892. MR2111728

[65] Degond, P. and Mas-Gallic, S. (1991), The weighted particle method for convection-difussion equations, Parts 1 & 2, Math. Comput. Vol. 53, pp. 485. MR983559 (90g:65126)

[66] DeVore, R. A. (2007), Optimal computation. International Congress of Mathematicians. Vol. I, pp. 187–215, Eur. Math. Soc., Zürich. MR2334191 (2008h:41005)

[67] DiPerna, R. J. and Lions, P. L. (1989), On the Cauchy problem for Boltzmann equations: Global existence and weak stability, Ann. Math. 130, 1989, 321-366. MR1014927 (90k:82045)

[68] DiPerna, R. J., Lions, P.-L. and Meyer, Y. (1991), L^p regularity of velocity averages Ann. Inst. H. Poincaré Anal. Non Lin. 8, pp. 271-288. MR1127927 (92g:35036)

[69] Donoho, D. L. (2006), Compressed sensing. IEEE Trans. Inform. Theory 52 (2006), no. 4, pp. 1289-1306. MR2241189 (2007e:94013)

[70] Douglas, J. (1931), Solution of the problem of Plateau, Trans. Amer. Math. Soc. v. 33, pp. 263-321. MR1501590

[71] E, W. and Engquist, B. (2003), The heterogeneous multiscale methods, Commun. Math. Sci. 1, pp. 87-132. MR1979846 (2004b:35019)

[72] Efendiev, Y. and Hou, T.-Y. (2009), Multiscale Finite Element Methods. Theory and Applications, Surveys and Tutorials in the Appl. Math. Sci., v4, Springer. MR2477579 (2010h:65224)

[73] Ekeland, I. and Témam, R. (1999), Convex Analysis and Variational Problems, Classics in Appl. Math., v28, SIAM. MR1727362 (2000j:49001)

[74] Engquist, B. and Runborg, O. (2003), Computational high frequency wave propagation, Acta Numerica, v. 12, pp. 181-266. MR2249156 (2007f:65043)

[75] Evans, L. (1988), Weak Convergence Methods for Nonlinear Partial Differential Equations, CBMS, Amer. Math. Soc. 74. MR1034481 (91a:35009)

[76] Evans, L. (1998), Partial Differential Equations, Grad. Text Math Vol. 19. Amer. Math. Soc. MR1625845 (99e:35001)

[77] Eymard, R., Gallouët, T. and Herbin, R. (2001), Finite volume approximation of elliptic problems and convergence of an approximate gradient, Applied Numerical Math. v. 37(1-2), pp. 31-53. MR1825115 (2003c:65118)

[78] Filbet, F. (2006), A finite volume scheme for the Patlak-Keller-Segel chemotaxis model, Numer. Math. 104(4), pp. pp. 457-488. MR2249674 (2007e:92002)

[79] Fjordholm, U., Mishra, S. and Tadmor, E. (2012), ENO reconstruction and ENO interpolation are stable, Found. of Comp. Math., in press.

[80] Francis, J. G. F. (1961), The QR transformation: a unitary analogue to the LR transformation. I., and The QR transformation. II., Comput. v. 4, pp. 265-271 and Comput. v. 4, pp. 332-345. MR0130111 (23:B3143)

[81] Friedman, A. (1964), Partial Differential Equations of Parabolic Type, Prentice Hall. MR0181836 (31:6062)

[82] Gear, C. W. (1973), Numerical Initial Value Problems in Ordinary Differential Equations. Prentice-Hall, Englewood Cliffs, NJ. MR0315898 (47:4447)

[83] Gelfand, I. M. and Fomin, S. V. (1963), Calculus of Variations, Dover. MR0160139 (28:3353)

[84] Gérard, P. (1991), Microlocal defect measures, Comm. Partial Differential Eqs 16, pp. 1761-1794. MR1135919 (92k:35027)

[85] Giles, M. B. and Süli, E. (2002), Adjoint methods for PDEs: a posteriori error analysis and postprocessing by duality, Acta Numerica, Vol. 11, pp. 145-236. MR2009374 (2005d:65190)

[86] Glimm, J. (1965), Solutions in the large for nonlinear hyperbolic systems of equations, Comm. Pure App. Math., 18, pp. 697-715. MR0194770 (33:2976)

[87] Glimm, J., Grove, J. W., Li, X. L. and Zhao, N. (1999), Simple front tracking, Contmp. Math., v.238, pp. 133-149. MR1724660 (2000h:76135)

[88] Gilbarg, D. and Trudinger, N. S. (1977), Elliptic Partial Differential Equations of Second Order, Springer-Verlag. MR0473443 (57:13109)

[89] Godunov, S. K. (1959), A difference scheme for numerical computation of discontinuous solutions of equations of fluids dynamics, Math. Sb., Vol. 47, pp. 271-290. MR0119433 (22:10194)

[90] Godlewski, E. and Raviart, P.-A. (1996), Numerical Approximation of Hyperbolic Systems of Conservation Laws, Appl. Math Sci. v 118, Springer. MR1410987 (98d:65109)

[91] Golse, F., Lions, P-L., Perthame, B. and Sentis, R. (1988), Regularity of the moments of the solution of a transport equation, J. Funct. Anal. 76, pp. 110-125. MR923047 (89a:35179)

[92] Golub, G. H. and Van Loan, C. (1996), Matrix Computations, 3rd Edition, Johns Hopkins Studies in Mathematical Sciences. MR1417720 (97g:65006)

[93] Gottlieb, D. and Orszag, S. (1977), Numerical analysis of spectral methods: theory and applications, CBMS-NSF Regional Conference Ser. Appl. Math., SIAM, Philadelphia, 1977. MR520152 (58:24983)

[94] Greengard, L. and Rokhlin, V. (1987), A fast algorithm for particle simulations, Journal of Computational Physics, 73(2), pp. 325-348. MR918448 (88k:82007)

[95] Gustasfsson, B., Kreiss, H.-O., and Oliger, J. (1995), Time dependent problems and difference methods, Wiley-interscinece. MR1377057 (97c:65145)

[96] Hairer, E., Nørsett, S. P. and Wanner, G. (1993), Solving ordinary differential equations I: Nonstiff problems, second edition, Springer Verlag, Berlin. MR1227985 (94c:65005)

[97] Hairer, E. and Wanner, G. (1996), Solving ordinary differential equations II: Stiff and differential-algebraic problems, Springer Verlag, Berlin. MR1439506 (97m:65007)

[98] Hamilton, R. S. (1982), Three Manifolds with Positive Ricci Curvature, J. Diff. Geom. Vol. 17, pp. 255-306. MR664497 (84a:53050)

[99] Han, Q. and Lin, F.-H. (1997), Elliptic Partial Differential Equations, Courant Lecture Notes, v.1, Amer. Math. Soc., Providence. MR1669352 (2001d:35035)

[100] Harten, A. (1983), High resolution schemes for hyperbolic conservation laws. J. Comput. Phys., v. 49, pp. 357-393. MR701178 (84g:65115)

[101] Harten, A. (1989), ENO schemes with subcell resolution, J. Comput. Phys. v. 83(1), pp. 148-184. MR1010163 (90i:76010)

[102] Harten, A., Engquist, B., Osher, S. and Chakravarthy, S. R. (1987), Uniformly high order accurate essentially non-oscillatory schemes. III, J. Comput. Physics 71, pp. 231-303. MR897244 (90a:65199)

[103] Hesthaven, J. S., Gottlieb, S. and Gottlieb, D. (2007), Spectral Methods for Time-Dependent Problems, Cambridge Monographs on Applied Comput. Math. v. 21, Cambridge Univ. Press, Cambrigde, UK. MR2333926 (2008i:65223)

[104] Hillen, T. and Painter, K. J. (2009), A User's Guide to PDE Models for Chemotaxis, J. Math. Biology, v. 58, pp. 183-217. MR2448428 (2009m:92017)

[105] Holden, H., and Risbero, N. H. (2002), Front Tracking for Hyperbolic Conservation Laws, Springer. MR1912206 (2003e:35001)

[106] Horstman, D. (2003), From 1970 until now: The Keller Segel model in chemotaxis and its consequences I, Jahresber DMV 105, pp. 103-169 and (2004) 106, pp. 51-69. MR2073515 (2005b:92005)

[107] Hou, T. Y. and Lax, P. (1991), Dispersive approximations in fluid dynamics, Comm. Pure and Appl. Math., v. 44, pp. 1-40. MR1077912 (91m:76088)

[108] Hou, T. Y., Li, C., Shi, Z., Wang, S. and Yu, X. (2011), On dingularity formation of a nonlinear nonlocal system, Arch. Rat. Mech. Anal. v. 199, pp. 117-144. MR2754339 (2012c:35184)

[109] Hou, T. Y. and Wu, X. H. (1997), A multiscale finite element method for elliptic problems in composite materials and porous media. J. Comput. Phys., v. 134, pp. 169-189. MR1455261 (98e:73132)

[110] Hughes, T. J. R. (2000), The Finite Element Method: Linear Static and Dynamic Finite Element Analysis, Dover Civil and Mechanical Engineering. MR1008473 (90i:65001)

[111] Hwu W. W.-M. (2011), GPU Computing Gems, Elseveir.

[112] Itô, K. (1983), Foundations of stochastic differential equations in infinite dimensional spaces, CBMS Notes, SIAM, Baton Rouge. MR771478 (87a:60068)

[113] Jaswon, M. A. (1963), Integral equation methods in potential theory. I, Proc. Royal Soc. London Series A, v. 275(1360) pp. 23-32; MR0154075 (27:4034)

[114] Johnson, C. (1988), Numerical Solution of Partial Differential Equations by the Finite Element Method, Cambridge University Press, New York. MR925005 (89b:65003a)

[115] Johnson, C. and Thomée, V. (1975), Error Estimates for a Finite Element Approximation of a Minimal Surface, Math. Comp. v.29, pp. 343-349. MR0400741 (53:4571)

[116] Kalnay, E. (2002), Atmospheric Modeling, Data Assimilation and Predictability, Cambridge University Press.

[117] Karmarkar, N. (1984), A New Polynomial Time Algorithm for Linear Programming, Combinatorica, Vol 4, nr. 4, p. 373-395. MR779900 (86i:90072)

[118] Karatzas, I. and Shreve, S. E. (1998), Methods of Mathematical Finance. Applications of Mathematics, v. 39. Springer-Verlag, New York. MR1640352 (2000e:91076)

[119] Keller, E. F. and Segel, L. A. (1971), Model for chemotaxis. J. Theor Biol, 30(2), pp. 225-234.

[120] Kevrekidis, I. G., Gear, W., Hyman, J. M., Kevrekidis, G., Runborg O. and Theodoropoulos, C. (2003), Equation-Free Multiscale Computation: enabling microscopic simulators to perform system-level tasks, Comm. Math. Sciences 1(4) pp. 715-762. MR2041455 (2005a:65075)

[121] Kohn, R. V. (2007), Energy-driven pattern formation. Inter. Congress Math. Vol. I, pp. 359-383, Eur. Math. Soc., Zürich. MR2334197 (2008k:49049)

[122] Kreiss, H.-O. (1964), On difference approximations of the dissipative type for hyperbolic differential equations, Comm. Pure Appl. Math. v. 17, pp. 335-353. MR0166937 (29:4210)

[123] Kreiss H.-O. and Oliger, J. (1972), Comparison of Accurate Methods for the Integration of Hyperbolic Equations, Tellus, v. 24, pp. 199-215. MR0319382 (47:7926)

[124] Kreiss, H.-O. and Lorenz, J. (2004), Initial-Boundary Value Problems and the Navier–Stokes Equations, Academic Press. MR998379 (91a:35138)

[125] Krylov, N. V. (1997), Lectures on Elliptic and Parabolic Equations in Holder Spaces, Graduate Studies in Math., v. 12, Amer. Math. Soc., Providence. MR1406091 (97i:35001)

[126] Kurganov, A. and Tadmor, E. (2000), New high resolution central schemes for nonlinear conservation laws and convection-diffusion equations, J. Comput. Physics, v. 160, pp. 241-282. MR1756766 (2001d:65135)

[127] Küther, M. and Ohlberger, M. (2003), Adaptive Second Order Central Schemes on Unstructured Staggered Grids, Proc. Ninth Intl. Conference Hyperbolic Problems, (T. Hou and E. Tadmor, eds), Springer-Verlag, pp. 675-684. MR2053216

[128] Lax, P. D. (1954), Weak solution of nonlinear hyperbolic equations and their numerical computation, Comm. Pure Appl. Math. 7, pp. 159-193. MR0066040 (16:524g)

[129] Lax, P. D. (1978), Accuracy and resolution in the computation of solutions of linear and nonlinear equations, "Recent advances in Numerical Analysis", Proc. Symp. Math. Res. Ctr., Univ. of Wisconsin, Academic Press, pp. 107-117. MR519059 (80b:65147)

[130] Lax, P. D. (1986), On dispersive difference schemes, Phys. D, 18, pp. 250-254. MR838330 (87h:65155)

[131] Lax, P. D. (2006), Hyperbolic Partial Differential Equations, Courant Lecture Notes, v.14, Amer. Math. Soc., Providence. MR2273657 (2007h:35002)

[132] Lax, P. D. and Nirenberg, L. (1966), On stability for difference schemes: A sharp form of Gàrding's inequality, Comm. Pure Appl. Math. v. 19, pp. 473-492. MR0206534 (34:6352)

[133] Lax, P. D. and Richtmyer, R. D. (1956), Survey of the stability of linear finite difference equations. Comm. Pure Appl. Math. 9, pp. 267-293. MR0079204 (18:48c)

[134] Lax, P. D. and Wendroff, B. (1960), Systems of conservation laws, Commun. Pure Appl Math. v. 13(2), pp. 217-237. MR0120774 (22:11523)

[135] van Leer, B. (1979), Towards the ultimate conservative difference scheme. V. A second-order sequel to Godunov's method, J. Comput. Phys. 32, 101–136.

[136] LeVeque, R. J. (2002), Finite Volume Methods for Hyperbolic Problems, Cambridge texts in Appl. Math. MR1925043 (2003h:65001)

[137] Levy, D. and Tadmor, E (1997), Non-oscillatory central schemes for the incompressible 2-D Euler equations, Mathematical Research Letters 4 (3), 1997, 321-340. MR1453063 (99a:65100)

[138] Lions, P. L. (1984), The concentration-compactness principle in the calculus of variations. The locally compact case, part 1. Annales de l'institut Henri Poincaré (C) Analyse non linéaire, 1 no. 2, pp. 109-145. MR778970 (87e:49035a)

[139] Lions, P. L. (1996), Mathematical Topics in Fluid Mechanics: Volume 1 - Incompressible Models, Oxford Lecture Series in Mathematics and Its Applications. MR1422251 (98b:76001)

[140] Lions, P. L. (1998), Mathematical Topics in Fluid Mechanics: Volume 2 -Compressible Models, Oxford Lecture Series in Mathematics and Its Applications, Oxford University Press. MR1637634 (99m:76001)

[141] Liu, X.-D., Osher, S. and Chan, T. (1994), Weighted essentially non-oscillatory schemes. J. Comput. Phys. v. 115(1), pp. 200-212. MR1300340

[142] Liu, Y.-J., Shu, C.-W., Tadmor E. and Zhang, M. (2007), Central discontinuous Galerkin methods on overlapping cells with a non-oscillatory hierarchical reconstruction, SIAM J. Numer. Anal., Vol. 45(6), pp. 2442-2467 MR2361897 (2009a:65256)

[143] Majda, A., McDonough, J. and Osher, S. (1978), The Fourier method for nonsmooth initial data, Math. Comp. 32(144) pp. 1041–1081. MR501995 (80a:65197)

[144] Majda, A. and Bertozzi A. (2001), Vorticity and Incompressible Flow, Cambridhe texts Appl. Math.

[145] Majda, A. (2003), Introduction to PDEs and Waves for the Atmosphere and Ocean, Courant Lecture Notes, vol 9., AMS. MR1965452 (2004b:76152)

[146] Majda, A., Abramov, R. V. and Grote, M. J. (2005), Information Theory and Stochastics for Multiscale Nonlinear Systems, CRM monograph series 25, American Mathematical Society. MR2166171 (2006k:76110)

[147] Mas-Gallic, S. and Raviart, P.-A. (1987), A particle method for first order symmetric systems, Numer. Math. 51, pp. 323-352. MR895090 (88d:65132)

[148] MATLAB - The Language of Technical Computing, http://www.mathworks.com/products/matlab/.

[149] Meyer, Y. (1993), Wavelets: Algorithms and Applications, Society Industrial Appl. Math. (SIAM), Philadelphia, PA. MR1219953 (95f:94005)

[150] Meyers, N. and Serrin, J. (1964), $H = W$, Proc. Nat, Acad. Sci. USA 51, pp. 1055-1056. MR0164252 (29:1551)

[151] Mock, M. S. and Lax, P. D. (1978), The computation of discontinuous solutions of linear hyperbolic equations, Comm. Pure Appl. Math. Vol. 31, pp. 423-430. MR0468216 (57:8054)

[152] Moore, G. E. (1965), Cramming more components onto integrated circuits, Electronics, v. 38 (8).

[153] Morgan, J. and Tian G. (2007), Ricci Flow and the Poincare Conjecture, Clay Mathematics Monographs. MR2334563 (2008d:57020)

[154] Murry, J. D. (2002), Mathematical Biology, Vols I & II, Springer.

[155] Nessyahu, H. and Tadmor, E. (1990), Non-oscillatory central differencing for hyperbolic conservation laws, J. Comput. Physics 87, pp. 408-463. MR1047564 (91i:65157)

[156] von Neumann, J. (1949), A letter to V. Bush, in "John von Neumann: selected letters", Redei M. ed., London Math. Soc. and Americam Math. Soc., History of Mathematics, Vol. 27.

[157] Nochetto, R., Siebert K. G. and Veeser A. (2009), Theory of Adaptive Finite Element Methods: an Introduction, Multiscale, Nonlinear and Adaptive Approximation, (R. DeVore and A. Kunoth eds), Springer (2009), 409-542. MR2648380 (2011k:65164)

[158] Oberman, A. (2008), Wide stencil finite difference schemes for the elliptic Monge–Ampere equation and functions of the eigenvalues of the Hessian, DCDS Ser. B 10(1), pp. 221-238. MR2399429 (2009f:35101)

[159] Orszag, S. (1971), Numerical simulation of incompressible flows within simple boundaries. I, Studies in Applied Math. v. 50, pp. 293-327. MR0305727 (46:4857)

[160] Osher, S. J. and Sethian, J. A. (1998), Fronts propagating with curvature-dependent speed: algorithms based on Hamilton–Jacobi formulations, J. Comput. Phys., 79, pp. 12-49. MR965860 (89h:80012)

[161] Osher, S. J. and Fedkiw, R. P. (2003), Level set methods and dynamic implicit surfaces, Appl. Math. Sci, v. 153, Springer. MR1939127 (2003j:65002)

[162] Patera, A. T. (1984), A Spectral Element Method for Fluid Dynamics: Laminar Flow in a Channel Expansion, J.Comput. Phys. v. 54, pp. 468-488.

[163] Pedlosky, J. (1987), Geophysical Fluid Dynamics, 2nd ed., Springer.

[164] Perelman, G. (2005), Ricci flow with surgery on three-manifolds, preprint, math.DG/0303109.

[165] Perona, P. and Malik, J. (1990), Scale-space and edge detection using anisotropic diffusion, Patt. Aanal. Mach. Intell. 12(7), pp. 629-639.

[166] Perthame, B. (2007), Transport equations in biology. Frontiers in Mathematics. Birkhäuser Verlag, Basel. MR2270822 (2007j:35004)

[167] Peskin, C. S. (1977), Numerical analysis of blood flow in the heart, J. Comput. Phys. 25 pp. 220-252. MR0490027 (58:9389)

[168] Peskin, C. S. (2002), The immersed boundary method, Acta Numerica, 11, pp. 1-39. MR2009378 (2004h:74029)

[169] Quarteroni, A. (2007), Cardiovascular mathematics. International Congress of Mathematicians. Vol. I, pp. 479-512, Eur. Math. Soc., Zürich. MR2334201 (2008f:92021)

[170] Radó, T. (1933), On the Problem of Plateau, Ergeben. d. Math. u. ihrer Grenzgebiete. Berlin: Springer-Verlag, 1933.

[171] Rauch, J. (2012), Hyperbolic Partial Differential Equations and Geometric Optics, Amer. Math. Soc. Graduate Text, v. 133. MR2918544

[172] Raviart, P.-A. (1984), An analysis of particle methods, in Numerical Methods in Fluid Dynamics, vol. 1127 of Lecture Notes in Mathematics, Springer, Berlin, New York, pp. 243-324. MR802214 (87h:76010)

[173] Reed W. H. and Hill, T. R. (1973), Triangular mesh methods for the neutron transport equation, Tech. Report LA-UR-73-479, Los Alamos Sci. Lab.

[174] Richardson, L. F. (1922), Weather Prediction by Numerical Process, Cambridge University Press, xii+236 pp. Reprinted by Dover Publications, New York, 1965. MR2358797 (2008g:86013)

[175] Richtmyer, R. and Morton K. W. (1967), Difference methods for initial-value problems, Wiley, reprinted by Krieger Publ. Co., Florida, 1994. MR1275838 (95b:65003)

[176] Rizzo, F. J. (1967), An integral equation approach to boundary value problems of classical elastostatics, Quarterly of Appl. Math., v. 25, pp 83.

[177] Roe, P. L. (1981), Approximate Riemann solvers, parameter vectors, and difference schemes, J. Comput. Phys. v. 43(2), pp. 357-372. MR640362 (82k:65055)

[178] Rudin, L., Osher, S. and Fatemi, E. (1992), Nonlinear total variation based noise removal algorithms, Physica D, 60, 259-268.

[179] Saad, Y. (2003), Iterative Methods for Sparse Linear Systems, 2nd edition, SIAM, Philadelphia. MR1990645 (2004h:65002)

[180] Samarskii, A. A. (1965), On monotone difference schemes for elliptic and parabolic equations in the case of a non-selfadjoint elliptic operator, Zh. Vychisl. Mat. i. Mat. Fiz. v. 5, pp. 548-551 (Russian). MR0189275 (32:6702)

[181] Samarskii, A. A. (1971), Introduction to the Theory of Difference Schemes, Nauka, Moscow (Russian). MR0347102 (49:11822)

[182] Serre, D. (1999), Systems of Conservation Laws, Vol. 1&2, Cambridge Univ. Press. MR1707279 (2000g:35142)

[183] Sethian, J. A. (1999), Level Set Methods and Fast Marching Methods: Evolving Interfaces in Computational Geometry, Fluid Mechanics, Computer Vision and Materials Science, Cambridge University Press. MR1700751 (2000c:65015)

[184] Sethian, J. A. (1999), Fast Marching Methods, SIAM Review, 41(2), pp. 199-235. MR1684542 (2000m:65125)

[185] Shreve, S. E. (2004), Stochastic calculus for finance. vols I & II. Springer-Verlag, New York.

[186] Shu, C.-W. and Osher, S. (1989), Efficient implementation of essentially nonoscillatory shock-capturing schemes. II. J. Comput. Phys. v. 83(1), pp. 32-78. MR1010162 (90i:65167)

[187] Smoller, J. (1994), Shock waves and Reaction-Diffusion Equations, 2nd edition, v. 258, Springer. MR1301779 (95g:35002)

[188] Souganidis. P. (1985), Approximation schemes for viscosity solutions of Hamilton–Jacobi equations, Journal of Differential Equations, v. 57, pp. 1–43. MR803085 (86k:35028)

[189] Strang, G. (1964), Accurate partial difference methods. II. Non-linear problems. Numer. Math. v. 6, pp. 37-46. MR0166942 (29:4215)

[190] Strang, G. and Fix, G. J. (1973), An Analysis of the Finite Element Method, Prentice-Hall, Inc., Englewood Cliffs, NJ. MR0443377 (56:1747)

[191] Struwe, M. (2008), Variational Methods, Springer. MR2431434 (2009g:49002)

[192] Sweby, P. (1984), High-resolution schemes using flux limiters for hyperbolic conservation-laws, SIAM J. Numer. Analysis, v. 21, pp. 995-1011, MR760628 (85m:65085)

[193] Symm, G. T. (1963), Integral equation methods in potential theory. II, Proc. Royal Soc. London A, v. 275(1360), pp. 33-46. MR0154076 (27:4035)

[194] Szabo, B. and Babuška, I. (1991), Finite Element Method Analysis, John Wiley, New-York.

[195] Tadmor, E. (1989), Convergence of spectral methods for nonlinear conservation laws, SIAM J. Numer. Anal. Vol. 26, pp. 30-44. MR977947 (90e:65130)

[196] Tadmor, E. (1991), Local error estimates for discontinuous solutions of nonlinear hyperbolic equations, SIAM J. Numer. Anal., Vol. 28 (4), pp. 891-906. MR1111445 (92d:35190)

[197] Tadmor, E. (2002), High resolution methods for time dependent problems with piecewise smooth solutions, in "International Congress of Mathematicians", Proc. the ICM02 Beijing 2002 (Li Tatsien, ed.), Vol. III: Invited lectures, Higher Education Press, pp. 747-757. MR1957576 (2003m:65150)

[198] Tadmor, E. (2003), Entropy stability theory for difference approximations of nonlinear conservation laws and related time dependent problems, Acta Numerica v. 12, pp. 451-512. MR2249160 (2007g:35150)

[199] Tadmor, E. (2007), Filters, mollifiers and the computation of the Gibbs phenomenon, Acta Numerica, v. 16, pp. 305-378. MR2417931 (2009c:65033)

[200] Tadmor, E., Nezzar, S. and Vese, L. (2004), A multiscale image representation using hierarchical (BV,L2) decompositions Multiscale Modeling and Simulations 2(4), pp. 554-579. MR2113170 (2005h:68163)

[201] Tadmor, E. and Zhong, W. (2007), Energy-preserving and stable approximations for the two-dimensional shallow water equations, Proc. the 2006 Abel Symposium, "Mathematics and Computation, a Contemporary View", Norway, May, 2006. MR2503502 (2010e:76090)

[202] Tadmor, E. and Tao, T. (2007), Velocity averaging, kinetic formulations and regularizing effects in quasilinear PDEs, Comm. Pure & Applied Math. 60, pp. 1488-1521. MR2342955 (2008g:35011)

[203] Tao, T. (2006), Perelman's proof of the Poincare conjecture: A nonlinear PDE perspective, preprint, arXiv:math.DG0610903. MR2256586

[204] Tao, T. (2006), Nonlinear Dispersive Equations, CBMS Vol. 106, Amer. Math. Soc. MR2233925 (2008i:35211)

[205] Tartar, L. (1979), Compensated compactness and applications to partial differential equations, Research Notes in Math., 39, pp. 136-210. MR584398 (81m:35014)

[206] Tartar, L. (1990), H-measures, a new approach for studying homogenization and concentration effects in partial differential equations. Proc. Roy. Soc. Edinburgh Sect. A, 115 no. 3-4, pp. 193-230. MR1069518 (91h:35042)

[207] Taylor, M. (1996), Partial Differential Equations, Appl. Math. Sci. vol I, II and III, Springer. MR1395147 (98b:35002a)

[208] Temlyakov, V. N. (2006), Greedy approximations, Foundations of Comput. Math. (FoCM), Santander 2005, pp. 371-394, London Math. Soc. Lecture Note Ser., 331, Cambridge Univ. Press, Cambridge. MR2277112 (2007k:41046)

[209] Thomée, V. (1969), Stability theory for partial difference operators, SIAM Rev. 11 pp. 152-195. MR0250505 (40:3739)

[210] Tian, G. (2002), Geometry and nonlinear analysis. Proc. Inter. Congress Math., Vol. I (Beijing, 2002), pp. 475-493, Higher Ed. Press, Beijing2. MR1989199 (2004j:53052)

[211] Tikhonov A. N. and Samarskii, A. A. (1962), Homogeneous difference schemes on nonuniform nets Zh. Vychisl. Mat. i. Mat. Fiz. 2, 812-832 (Russian). MR0168128 (29:5392)

[212] Toro, E. F. (1999), Riemann solvers and numerical methods for fluid dynamics. A practical introduction. Second edition. Springer-Verlag, Berlin. MR1717819 (2000f:76091)

[213] Toselli, A. and Widlund, O. (2004), Domain Decompposition Methods - Algorithms and Theory, Springer Series in Computational Mathematics, v. 34. MR2104179 (2005g:65006)

[214] Trefethen, L. N. (2000), Spectral Methods in Matlab, SIAM. MR1776072 (2001c:65001)

[215] Trefethen, L. N. and Bau, D. (1997), Numerical Linear Algebra, SIAM. MR1444820 (98k:65002)

[216] Turkel, E. (1999), Pre-conditioning Techniques in Computational Fluid Dynamics, Annual Reviews in Fluid Mechanics 1999, V. 31, 385-416. MR1670946 (99k:76120)

[217] Venakides, S. (1990), The Korteweg-de Vries equation with small dispersion: higher order Lax–Levermore theory, Comm. Pure and Appl. Math., v. 43(3) pp. 335-361. MR1040144 (91k:35236)

[218] Villani, C. (2003), Topics in Optimal Transportation, Grad. Course Math., Amer. Math. Soc. Vol. 58. MR1964483 (2004e:90003)

[219] Wesseling, P. (2004), An Introduction to Multigrid Methods, R.T. Edwards Inc. Philadel-
     phia.
[220] Xu, J. and Zikatanov, L. (2002), The method of alternating projections and the method of
     subspace corrections in Hilbert space, J. Amer. Math. Soc. v. 15 pp. 573-597. MR1896233
     (2003f:65095)
[221] Zhang, Y.-T., Chen, S., Li, F., Zhao, H. and Shu, C.-W. (2011), Uniformly accurate dis-
     continuous Galerkin fast sweeping methods for Eikonal equations, SIAM J. Scie. Comput.,
     v33(4), pp. 1873-1896. MR2831038

DEPARTMENT OF MATHEMATICS AND INSTITUTE FOR PHYSICAL SCIENCE & TECHNOLOGY, CEN-
TER OF SCIENTIFIC COMPUTATION AND MATHEMATICAL MODELING (CSCAMM), UNIVERSITY OF
MARYLAND, COLLEGE PARK, MARYLAND 20742

  E-mail address: `tadmor@cscamm.umd.edu`

  URL: `http://www.cscamm.umd.edu/tadmor`